1-1-2013

Aspect Ratio Effect on Melting and Solidification During Thermal Energy Storage

Prashanth Sridharan
University of South Florida, psridha2@mail.usf.edu

Aspect Ratio Effect on Melting and Solidification During Thermal Energy Storage

by

Prashanth Sridharan

A thesis submitted in partial fulfillment
of the requirements for the degree of
Master of Science in Mechanical Engineering
Department of Mechanical Engineering
College of Engineering
University of South Florida

Co-Major Professor: Muhammad Rahman, Ph.D.
Co-Major Professor: Yogi Goswami, Ph.D.
Elias Stefanakos, Ph.D.

Date of Approval:
July 3, 2013

Keywords: Latent Heat, Natural Convection
Phase Change Material, Sodium Nitrate, Vertical Cylinder

ACKNOWLEDGMENTS

Antonio and Dr. Rahman

TABLE OF CONTENTS

LIST OF TABLES....ii

LIST OF FIGURES....iii

ABSTRACT....iv

CHAPTER 1: INTRODUCTION....1

CHAPTER 2: MATHEMATICAL MODELS....13
- 2.1 Governing Equations and Boundary Conditions....13
- 2.2 Numerical Modeling and Computation....15

CHAPTER 3: RESULTS AND DISCUSSION....20
- 3.1 Melting Results....20
- 3.2 Solidification Results....31

CHAPTER 4: CONCLUSIONS....48

REFERENCES....50

APPENDICES....54
- Appendix A Nomenclature....55

LIST OF TABLES

Table 1 Details of cylinder cases.....35

Table 2 Simulation results-present study vs validation study.....42

LIST OF FIGURES

Figure 1 Cylinder schematic..... 19

Figure 2 Transient melt fraction of first six cases.....36

Figure 3 Transient melt fraction of last four cases..... 36

Figure 4 Melt time vs aspect ratio.....37

Figure 5 Case 2 stream function and temperature distribution contours at various melt fractions..... 38

Figure 6 Case 9 stream function and temperature distribution contours at various melt fractions..... 39

Figure 7 Transient heat flux of various cases during melting 39

Figure 8 Distribution of θ for various cases..... 40

Figure 9 Dimensionless transient melt fraction of first seven cases.....40

Figure 10 Dimensionless transient melt fraction of cases 8 and 9.....41

Figure 11 Comparison with validation study [21]..... 43

Figure 12 Transient melt fraction of various cases during solidification..... 43

Figure 13 Case 2 temperature distribution and stream function contours at various melt fractions during solidification.....44

Figure 14 Case 9 temperature distribution and stream function contours at various melt fractions during solidification..... 44

Figure 15 Cases 2 and 9 melt distribution at various melt fractions during solidification.....45

Figure 16 Transient heat flux curve during solidification.....46

Figure 17 95% solid fraction time vs aspect ratio.....46

Figure 18 Percent of max time vs aspect ratio.....47

ABSTRACT

The present work investigates, numerically, the process of melting and solidification in hollow vertical cylinders, filled with air and phase change material (PCM). The PCM used is sodium nitrate, which expands upon melting. Therefore, a void must be present within the cylinder, which is filled with air. The influence of cylinder shape on melting time is determined. The numerical model takes both conductive and convective heat transfer into account during the melting process. The Volume-of-Fluid (VOF) model is used to track the interface between the PCM and air as the PCM melts. Three dimensionless numbers represent the characteristics of the problem, which are the Grashof, Stefan, and Prandtl numbers. The Stefan and Prandtl numbers are held constant, while the Grashof number varies. Inner Aspect Ratio (AR) is used to characterize the shape of the cylinder, which is defined as the ratio of the height to the diameter of the vertical cylinder. In this study, a range of AR values from 0.23 to 10 is investigated. Cylinders with small AR, corresponding to high Grashof numbers, lead to lower melting times compared with cylinders with high AR. The molten PCM velocity was also influenced greatly by this difference between solid PCM shape between high and low AR cases. Cylinders with small AR, corresponding to high Grashof numbers, lead to higher solidification times compared with cylinders with high AR. It was found that the velocity decreased during the solidification process, but the shape of the cylinder had an effect on the decrease. Natural convection velocity

was found to decrease during the solidification process and, therefore, its effects diminish as solidification proceeds.

CHAPTER 1: INTRODUCTION

Alternative and renewable energies are vital in supplementing some/all of the required energy for the growth and sustainability of a large world population. Some of these such as solar or wind energy, have an intermittent energy source, which creates the necessity for energy storage. Energy stored in the form of heat is called thermal energy storage. Thermal energy storage (TES) is not limited in application to renewable energies only. Storing heat can help offset peak/off-peak load demand of coal power plants, solar power plants, geothermal plants, and any thermodynamic cycle incorporating the principle of converting thermal energy to electrical energy. A cogenerating thermodynamic cycle incorporating a Stirling cycle is an example.

TES systems can store this thermal energy in terms of sensible heat or latent heat. Sensible heat storage systems store heat through the material's heat capacity over a large temperature difference. Latent heat storage systems incorporate material's phase changes, in addition to the heat capacity, to store thermal energy. Materials used in latent heat storage systems are called Phase Change Materials (PCM). Phase change requires large changes in internal energy of the material. The large change in internal energy allows latent heat storage to have higher thermal storage density compared to sensible heat storage, while the temperature difference required is lower [10,35]. For example, 80 times as much energy is required to melt 1kg of ice compared to raising the temperature of 1kg of water by 1 ^{o}C [13]. Solar steam

generation for power plants requires latent heat storage systems for a steam saturation temperature range between 200-320 ^{o}C, which is valid for Solar parabolic trough technology [23].

Carbonate salt PCMs that can be applied in temperatures above 500 K (226 ^{o}C) are of interest in high temperature Brayton cycle turbines [14]. Nitrate salt PCMs are good candidates for Compact Linear Fresnel Reflector systems using low pressure turbines at or below 600 K (326 ^{o}C) [14]. High temperature PCM can also generate high enthalpy steam for better Rankine cycle performance [38]. There is also a need for PCMs in applications above 400 ^{o}C for storage of thermal energy for electrical energy generation in 100 MWe plants for 6 hours of more [38].

The various PCMs mentioned above can be encapsulated in different ways. They can be encapsulated in tubes to be used in tube heat exchangers. They can be macro-encapsulated in spheres, cylinders, and other geometric shapes to be used in packed bed heat exchangers. They can also be micro-encapsulated and embedded in a high conductive medium or in a fluidized bed. Each heat exchanger will have an optimized container size and dimensions for efficient heat transfer.

Assis et al. [3] investigated the melting process in a spherical shell both numerically and experimentally. They studied spheres of different diameters. The outer wall temperature of the sphere was kept constant and was allowed to vary 2-20 ^{o}C above the mean melting temperature of PCM. Through the parametric study, it was found that increasing the Stefan number decreased the total melt time. This also translated to larger heat fluxes at larger Stefan

Faraji and Hamid [11] numerically investigated melting in an rectangular enclosure with protruding heat sources. The energy dissipated from the heat sources is absorbed by the PCM, which is kept between the walls of the enclosure. The energy equation was solved using the

enthalpy method. The conservation equations were solved using finite difference method, which incorporated both conduction and natural convection heat transfer mechanisms. The authors concluded that the initial stages of the melting process, the lower PCM region is dominated by conduction. They also found that the average Nusselt number decreases as melting process progresses. This meant that the heat generated by the protruding heat sources was absorbed by the melting front, which causes the heat source temperature to stay constant.

Hosseini et al. [15] looked at the melting behavior of a PCM in a shell and tube heat exchanger. They investigated the effect of natural convection during the melting process. The phase change process was modeled using the enthalpy-porosity method. The authors determined the effect of increasing the heat transfer fluid's inlet temperature. They found that the total melting time is reduced by 63% when the inlet heat transfer fluid entered at 80 ^{o}C.

Hosseinizadeh et al. [16] numerically and experimentally investigated the performance of PCM-based heat sinks during melting and solidification. The effect on thermal management of heat sinks was investigated by comparing heat sinks with and without PCM. As the input power level was increased, the melting rate of the PCM increased as well. In the initial stages of the melting process, the heat transfer mode is conduction. As the melt region enlarges, natural convection slowly takes over as the primary heat transfer mode. The Volume of Fluid and enthalpy-porosity models are used to track the deformable interface and track the melting front respectively. It was found that the heat sinks with PCM stayed at a constant temperature during the period the PCM melted. After complete melting had occurred, the heat sinks with the PCM continued to increase in temperature, which is the same as the heat sinks without the PCM. The fins of the heat sinks played a great role for the heat sinks with PCM. As expected, increasing the

number of fins increased the melting rate of the PCM, which also kept the heat sinks at a lower temperature.

Ismail and Gracas E. da Silva [20] investigated the melting process of a PCM around a horizontal cylinder. The numerical model allowed for natural convection to be taken into account. The finite volume method was used to discretize the conservation equations. It was found that increasing the Stefan number decreased the total melt time. The authors also managed to develop correlations for the total melt volume in terms of the cylinder surface temperature, Rayleigh number, and Stefan number.

Kim et al. [22] investigated the melting process of a PCM numerically. The authors delved into the effect of the inclusion of a deformable liquid-gas interface on the melting process. The Volume of Fluid model was used to include the deformable interface. The enthalpy-porosity model was used to help simulate the melting process. If the deformable interface is included, the melting occurs quicker. It was noted that the increased melting rate was ascribed to an increase in total absorbed heat. The melting front contact area was allowed to widen with the inclusion of a deformable interface. Induced flow within the molten PCM also helped increase the heat transfer as the contact area widened.

El Omari et al. [9] investigated the influence of container shape on natural convection and melting in the containers. Five geometries of equal inner volume were inspected. These geometries included being rounded, rectangular, and thick or thin. The positions of the geometries were different such that they were either centered with respect to the cooled surface or positioned farther vertically upward. The shapes inspected include a half disc, rectangular with various width to length ratios, and oblong with rounded corners. The phase change is simulated by using the enthalpy-porosity method. Initially the melt front is similar in all the

shapes. As the melting process continues, it was found that the top portion of the PCM melted quicker than the bottom. The geometry that was shifted upward, which was also a thin geometry, had the highest velocity of the molten PCM. It was found that rounded corners helped the efficiency of heat transfer slightly.

Shatikian et al. [27] numerically investigated the effect of internal fin thickness on the melting process of a PCM-based heat sink. The top of the heat sink is exposed to open air. The heat sinks has fins to increase its efficiency, while the PCM is in between the fins. The authors found that melt fraction and Nusselt number had dependency on the product of the Stefan and Fourier numbers in the dimensionless analysis. They also found that the Rayleigh number should be included when dealing with thin fins. These thin fins allow the PCM layer to undergo natural convection, while the thick fins do not.

Tan et al. [30] investigated, numerically and experimentally, the effect of natural convection on constrained melting of PCM in spheres. The enthalpy-porosity model was used to calculate the phase change process. Fluent was used to characterize the transient melting front and the volume fraction during the melting process. The authors noted that thermal stratification occurs at the top of the sphere as the melting process progresses. This occurs due to the molten fluid rising to the top of the sphere, displacing the cold fluid below. It was also found that the numerical prediction increased in accuracy at the top of the sphere compared to the bottom. The cause was attributed to the support structure used to hold the sphere in the experimental setup. The structure caused chaotic perturbations at the bottom of the sphere, which affected the experimental data for the melting process.

Ye et al. [36] have investigated, numerically, the effect of cavity volume fractions of PCM on heat transfer and fluid flow. The numerical results were compared with published

numerical and experimental data for validation. The authors looked at the heat flux, total storage time, volume expansion ratio, liquid fraction, and velocity and temperature fields while varying the cavity volume fraction from 35% to 95%. It was found that increasing the cavity fraction causes the total storage time to increase.

Al-Abidi et al. [1] have investigated the solidification of a PCM triplex tube heat exchanger. The effect of the addition of fins, external or internal, on the charging and discharging process of the heat exchanger was looked at. It was found that fin thickness did not have an effect on solidification process, but thinner fins are preferred. Bauer investigated, numerically and analytically, the solidification process for flat plate and hollow cylinder geometries. The effective medium method was used to help solve the problem [4]. These geometries also incorporated fins to enhance heat transfer during solidification. It was found that numerical solutions matched analytical solutions when the dimensionless fin factor approached zero [4]. Guo and Zhang [12] investigated the effect of aluminum foils on the discharging process of a KNO_3-$NaNO_3$ high temperature latent heat storage system. It was found that the solidification time decreased from 54,504 seconds to 1756 seconds with proper incorporation of aluminum foil [12].

Ismail and Moraes [18] investigated, experimentally and numerically, the solidification process of various PCMs in spherical geometries. The material composition and thickness of the geometry was changed to inspect its effect on the solidification process. It was found that increasing the material thickness or increasing the sphere diameter led to larger solidification times. The primary heat transfer mode was conduction [18]. It was also found that the increase in diameter caused the convection in the liquid region, which moved the melt away from the solidified front, causing longer solidification times [18].

Ismail and Henríquez [19] investigated the solidification process in spheres numerically using the Finite difference method. The model used was a pure conduction model. The effects of material, thickness, sphere diameter, initial PCM temperature, and boundary condition temperature on the solidification process were studied. As expected, increasing the thickness or diameter increased solidification times [19]. Metals were found to enhance the heat transfer and decrease solidification times [19]. The internal radius of the spheres was kept constant, while the external radius was changed to change material thickness. It was found that for each shell material, there was a critical external radius value. If the external radius was increased to the critical value, decrease in solidification times were found, but increase in solidification times occurred when increasing the external radius past the critical value [19]. A decrease in the boundary condition temperature, or an increase in the initial PCM temperature, was found to decrease solidification times [19]. It was also found that an increase of the external surface Biot number caused decreases in solidification times [19].

Trp [32] experimentally and numerically investigated the melting and solidification process of paraffin wax in a shell and tube heat exchanger system. A two dimensional fully implicit FORTRAN code, based on control volume formulation, was used to numerically predict the heat transfer process [32]. It was found that natural convection did not have a large influence in the solidification process as the conduction heat transfer mechanism dominated [32]. It was found that solidification occurs first at the wall, after which it slowly progresses inside the container [32]. It was also found that the temperature curve moved downward as the solidification front progressed [32]. When larger Prandtl number value Heat Transfer Fluid (HTF) is used, the heat transfer process between the PCM and HTF gets slower [32].

Alawadhi investigated the process of solidification of water in an elliptical enclosure [2]. The finite element method and fixed grid techniques were utilized. The apparent heat capacity method was used to help simulate the phase change process. Natural convection was also included in the study. The ellipse aspect ratio, ellipse inclination, and initial water temperature were varied to determine their effect on the solidification process. It was found that total solidification time could be decreased by increasing the ellipse aspect ratio [2].

Tan et al. [31] investigated, numerically and experimentally, the solidification process of a PCM covering a tube transporting cryogenic nitrogen. They investigated the effect of various dimensionless numbers on the heat transfer and fluid flow. The Biot and Stefan numbers of the PCM, and the Stanton number of the nitrogen were found to play an important role. The authors found that the growth of the frozen PCM layer is sensitive to both the Biot and Stefan numbers. Large Biot and Stefan numbers cause fast growth rates of the frozen layer. Large Stanton number was found to cause a decrease in frozen layer thickness because a larger rise occurs in the coolant temperature. This was attributed to the coolant absorbing more heat at larger Stanton numbers.

Ye et al. [36]investigated the heat transfer and fluid flow of a plate-fin unit. Fluent was used to carry out the numerical simulation. The authors wanted to understand the effect of the temperature difference on the melting process. They found that increasing the temperature difference caused faster melting. This was attributed to higher heat fluxes at larger temperature differences. It was also found out that temperature differences larger than 20 ^{o}C did not greatly reduce the total melt time drastically. This is not true when temperature differences are under 20 ^{o}C. Cho and Choi [7] investigated experimentally the solidification of a mixture of water and paraffin wax in a spherical capsule. The inlet temperature was varied during the solidification

process. The inlet Reynolds number was also varied. The authors found the capsules on the periphery of the tank undergo phase change quicker than the capsules at the center of the tank. They found that the Reynolds number affected the melting process more than the solidification. This was attributed to the role of natural convection during the melting process.

Eames and Kamel [8] have experimentally studied the solidification process of water in spherical capsules used in thermal storage systems. Semi-empirical equations were used to help predict the ice mass in a sphere at any time. Dimensionless Fourier and Stefan numbers were used to help characterize the storage system. The authors found that most of the cold energy could be gotten from the capsules in 70% of the time required for complete discharge.

Ibrahim and Ahn [17] numerically investigated two dimensional axisymmetric solidification between two concentric cylinders. The authors used finite difference to solve the governing equations. The authors tested both explicit and implicit schemes in addition to varying number of nodes. The authors found that the explicit scheme gave more stable results compared to the implicit scheme. The inaccuracy encountered in the implicit scheme was attributed to arise from round of error. The authors suggest that the use of an alternate direction implicit scheme could help improve the results gotten from the implicit scheme.

Bilir and Ilken [6] numerically investigated solidification of PCM in cylinders and spheres under convection boundary condition. The enthalpy method was used during the formulation of the governing equations. The control volume approach was used to discretize and solve the governing equations. The Superheat Parameter, Biot number, and Stefan number were used to ascertain correlations of the solidification process. 9 values of the Superheat number, 21 values of the Stefan number, and 50 values of the Biot number were investigated to develop non-

dimensional correlations [6]. The correlations developed were found to have correlation coefficients higher than 0.996 implying good prediction.

Ramachandran et al. [26] numerically investigated the solidification process in a rectangular enclosure. The sides of the enclosure were kept at a constant temperature while the top and bottom walls were adiabatic. The governing equations were non-dimensionalized and solved using the alternate direction implicit finite difference scheme. The Boussinesq approximation is used. The influence of natural convection on solidification was found by studying high Rayleigh Number cases. The natural convection was found to strongly affect the shape of solid-liquid interface.

Shih and Chou [28] used an analytical iteration technique to model freezing a saturated liquid inside and outside spherical containers. The analytical iteration technique incorporates a transformation which transforms the diffusion equation into a convenient form. The success of this method depends on finding an appropriate transformation. The analytical scheme was compared with numerical solution. The scheme proved to be accurate with regard to the numerical solution.

Velraj et al. [33] numerically and experimentally investigated solidification of a PCM in a vertical tube. The incorporation of fins to enhance the heat transfer was investigated. The authors used implicit finite difference scheme to solve the governing equations. The enthalpy method was utilized as to characterize the solid-liquid interface. The heat flux at the inner wall of the tube with no fin had a sudden drop in magnitude, after which point it stayed low for the duration of the process. The incorporation of 8 fins decreased the total solidification time by 50% compared to the case with no fins. Fins are preferred for larger radius tubes.

The literature review presented above highlights studies done on the melting and solidification of phase change materials in various settings. Some of the authors above incorporated the enthalpy model and control volume discretization of the governing equations to simulate the melting and solidification process. Depending on the study, the authors investigated the influence of different variables on the melting and solidification process. The variables investigated include changes in boundary condition, initial condition, inlet heat transfer fluid temperature, and heat transfer fluid amongst others. The authors presented above that have studied cylindrical geometries have not considered the influence of cylinder shape.

The present study investigates aluminum vertical cylinders containing air and a PCM. The PCM used is Sodium nitrate, which has a melting point of 306 ^{o}C [5]. A numerical simulation of the melting, and solidification, process is done on the vertical cylinder. The air is present because a void space is required in the cylinder due to the volumetric expansion of Sodium Nitrate upon melting. An isothermal boundary condition is placed on the outside wall of the cylinder. The heat transfer mechanisms of conduction and natural convection are simulated. Natural convection is induced by density gradients in the molten Sodium Nitrate.

The uniqueness of this study is entangled with its purpose. The purpose of this study is to ascertain the effect of cylinder geometry on the melting and solidification process of Sodium Nitrate. The inner cylinder volume and Sodium Nitrate mass are held approximately constant in the present study. While the inner volume is held constant, the shape of the cylinder is allowed to change. This is done by changing the Inner Aspect Ratio (AR) of the cylinder, which is defined as the ratio of the inner height to inner diameter. This allows the cylinder shape to vary from tall, skinny, cylinders to short, fat, cylinders. Short, fat, cylinders have small heights and large diameters. Since the mass of Sodium Nitrate is held approximately constant, its total melting and

solidification time is directly controlled by the shape of the cylinder. The purpose of this study is to describe the geometrical effect of cylinder shape on the melting and solidification process of Sodium Nitrate.

CHAPTER 2: MATHEMATICAL MODELS

2.1 Governing Equations and Boundary Conditions

A vertical cylinder under the effect of a gravitational field is considered, shown in Figure 1. The problem is axisymmetric about the vertical axis of the cylinder. The radial axis is the y-axis and the vertical axis is the x-axis. As displayed, the vertical cylinder contains salt, which is the PCM, and air. The salt used for this study is sodium nitrate. The gravity vector acts in the negative x-direction. Ten cases are considered. All cases considered have a constant wall thickness of 0.5mm. Initially, the temperature of the system is such that the sodium nitrate is in the solid phase. The initial temperature is 576.95 K. There is a step change in temperature on the outer wall of the cylinder, which is modeled as an isothermal boundary condition. The assigned temperature is 10 K above the melting point of sodium nitrate. Heat transfer within the solid wall is by conduction. Heat transfer through the Sodium Nitrate and air occurs through both conduction and natural convection.

The following assumptions were made for the numerical simulation:

1. Sodium Nitrate and air are isotropic and homogeneous.
2. Air and molten Sodium Nitrate behave as Newtonian fluids.
3. The Boussinesq approximation can be used to describe the natural convection in the liquid phase.

4. Sodium nitrate density, thermal conductivity, specific heat, and viscosity are temperature dependent.
5. The initial temperature of the system is 576.95 K, which is below the melting/softening temperature of the Sodium Nitrate.
6. The melting of Sodium Nitrate takes place over an interval from 577.95 to 579.95 K; the density varies linearly in this region.
7. Air density can be approximated using the ideal gas model.
8. The flow is viscous and laminar.

The following material properties and input parameters were used in the simulation. The mushy zone temperature dependent density function of Sodium Nitrate is 66282.45 – 111T [5]. The liquid phase temperature dependent density function of Sodium Nitrate is 2628.5 – 1.2424T [5]. The temperature dependent dynamic viscosity function of Sodium Nitrate is 0.011916 - 0.00001533T [24]. The latent heat of fusion of Sodium Nitrate is 178000 J/kg [5]. The melting temperature of Sodium Nitrate is 579.95 K [5]. The temperature dependent specific heat function of Sodium Nitrate is 444.53 – 2.18T. The temperature dependent thermal conductivity of Sodium Nitrate is 0.305762 + 0.000447T [37]. The specific heat of Aluminum is 871 J/kg-K. The thermal conductivity of Aluminum is 202.4 W/m-K.

The governing equations for the problem are the conservation of mass, momentum and energy equations. The conservation of mass and momentum are shown below.

$$\frac{\partial}{\partial t}(\alpha_i \rho_i) + \nabla \cdot (\alpha_i \rho_i \boldsymbol{u_i}) = 0 \qquad [1]$$

where u_i, is the velocity vector of the i^{th} fluid. The linear momentum conservation equation can be expressed as:

$$\frac{\partial}{\partial t}(\alpha_i \rho_i \boldsymbol{u_i}) + (\boldsymbol{u_i} \cdot \nabla)(\alpha_i \rho_i \boldsymbol{u_i}) = -\alpha_i \nabla P + \alpha_i \rho_i \mathbb{F}_b + \alpha_i \mu \nabla^2 \boldsymbol{u_i} \qquad [2]$$

where F_b=-g, is the gravitational body force.

The volume fraction of the i^{th} fluid (α) which is defined as:

$$\alpha_i = \frac{volume\ of\ the\ phase\ in\ a\ cell}{volume\ of\ the\ cell} \quad [3]$$

The enthalpy method has been used to track the melting front of Sodium Nitrate. The temperature dependence of the energy equation is converted to enthalpy dependence. The transformed conservation of energy equation with enthalpy is shown below.

Transformed conservation of energy:

$$\frac{\partial}{\partial t}(\alpha_i \rho_i \hbar_i) + \nabla \cdot (\alpha_i \rho_i \boldsymbol{u_i} \hbar_i) = \alpha_i \left(\frac{\partial P}{\partial t} + \boldsymbol{u_i} \cdot \nabla P\right) + \alpha_i \nabla \cdot (\kappa_i \nabla T) \quad [4]$$

The melting simulation is carried out such that the final conditions (velocity, pressure, and temperature) of the melting simulation become the initial conditions of the solidification simulation. There is a step change in temperature on the outer wall of the cylinder, which is modeled as an isothermal boundary condition. The assigned temperature is 10 K above the melting point of Sodium Nitrate during the melting simulation. The boundary condition in the final data file from the melting simulation is changed to 10 K below the melting point of Sodium Nitrate. This simulation is continued using this data file to simulate the solidification process.

2.2 Numerical Modeling and Computation

An important note to understand is the numerical setup of the melting interval of Sodium Nitrate in FLUENT. Through use of the enthalpy-porosity model, the melting point of the PCM is input into FLUENT over a temperature range. Although it is known that Sodium Nitrate has a melting point at a specific temperature, it is simulated as melting over a range of 2 K. The benefit of the enthalpy-porosity model is that an explicit boundary condition is not needed at the solid-liquid interface to characterize its progression during the melting process [34]. This model also forces the velocities to zero when the melt fraction of a cell volume approaches 0. This is

done by incorporating a source term in the conservation of momentum equation. A Multiphase Volume-of-Fluid model is used in the simulation to simulate the deformable interface between the air and the PCM.

The vertical cylinder is discretized by a control volume approach. The governing equations for the conversation of mass, momentum, and energy are solved numerically on the discretized cylinder. The pressure-velocity equations were solved through Semi-Implicit Method for Pressure Linked Equations (SIMPLE) algorithm. A Multiphase Volume-of-Fluid model is used in the simulation to keep track of the interface between the Air and Sodium nitrate. The enthalpy-porosity model is used to keep track of the melting front of the Sodium nitrate. The transient formulation was First-Order Implicit. The Solution Control Under-Relaxation factors were 0.2, 0.7, 0.7, 0.4, 0.9, and 1 for pressure, density, body forces, momentum, liquid fraction update, and energy respectively. The domain was discretized using quadrilateral cells, where importance was given to the aspect ratio of the cell. A time step of 0.004 seconds was used for all cases. Solution convergence was checked during each time step, where the scaled absolute residuals were 10^{-3} for both continuity and momentum equations, and 10^{-6} for energy equation.

The SIMPLE algorithm is used to solve the pressure-velocity linked equations. A summary is given below, but a detailed analogue of the SIMPLE algorithm is given by Patankar [25]. The reason for using this algorithm is because the pressure and velocity fields are coupled with each other, while neither field is given. Since the pressure gradient is the driving force for flow, the pressure values are initially guessed. The velocity field is calculated such that the continuity equation is satisfied using the guessed pressure field. Therefore, to ensure accuracy, as the guessed pressure field approaches the realistic pressure field, the computed velocity field approaches the realistic velocity field as well. The guessed pressure field approaches the correct

pressure field through the addition of a pressure and velocity correction factors [25]. Patankar and others have developed a algorithm, which slowly corrects the guessed pressure and velocity fields to the correct fields, which is called the Semi-Implicit Method for Pressure-Linked Equations (SIMPLE) Algorithm [25].

The phase change aspect of our problem is considered through utilizing the enthalpy-porosity method. This method helps characterize and track the liquid-solid interface during the melting/solidification process. This model does not require an explicit condition to determine the liquid-solid interface, which is a bonus as well [34]. This is done through the incorporation of a new variable called the liquid fraction. It is assumed that the Sodium Nitrate melting behavior is characterized by a mushy zone. This mushy zone is to differentiate materials that melt at a single temperature versus those that melt in a range of temperatures. Normally, the amount of energy absorbed by a material, which does not change phase, is only due to sensible heat. Since there is phase change, the latent heat must also be taken into account. For the melting/solidification problem, the total enthalpy of the material, HH, is the sum of the sensible heat, h, and latent heat, ΔH, shown below.

$$HH = h + \Delta H \quad [5]$$

The sensible heat in the above equation is the product of the specific heat capacity of the material and the temperature increase it undergoes. Since enthalpy is temperature dependent, the Conservation of Energy Equation is transformed such that its temperature dependence is changed to enthalpy dependence. An additional equation is required to fully solve for the temperature distribution and the solid-liquid interface [34]. As mentioned before, the total enthalpy is the sum of the sensible and latent enthalpies. If the material is below its transition temperature, then the amount of energy it absorbs is only based on the sensible enthalpy. As the material changes

phase, it absorbs or releases energy. Before melting/solidification has occurred, the change in latent enthalpy is equal to zero. When melting/solidification has finished, the change in latent enthalpy is equal to the latent heat of phase change. In between these extremes, it is assumed that the change in latent enthalpy is proportional to the product of the liquid fraction and the latent heat of phase change. When the control volume is only solid, the liquid fraction is zero, which forces the latent enthalpy to zero. When the control volume has fully melted, the liquid fraction is one, which forces the latent enthalpy to equal the latent heat of phase change as expected. Using this definition, the liquid fraction can be solved for, which is shown in Equation below. The temperature field within the geometry is determined by iteration between the transformed Conservation of Energy and Liquid Fraction equations.

$$\alpha = \frac{\Delta H}{L} = \frac{T - T_{solidus}}{T_{liquidus} - T_{solidus}} \quad [6]$$

FLUENT sets the porosity within a computational volume/cell equal to the liquid fraction. When a cell is fully solid, the liquid fraction is zero, and hence is nonporous. As the liquid fraction increases, the computational cell is treated as a porous material. When the liquid fraction is one, the cell has 100% porosity. FLUENT incorporates a momentum source term within the conservation of momentum equation to help force the velocities to zero. The mushy zone constant helps characterize the velocity damping effect as the material solidifies. This constant is set to a value such that flow occurs easily at high liquid fractions, but forces velocities to zero as the liquid fraction approaches zero [34]. Usually, the value of this constant is in the range of 10^4 to 10^7 [1].

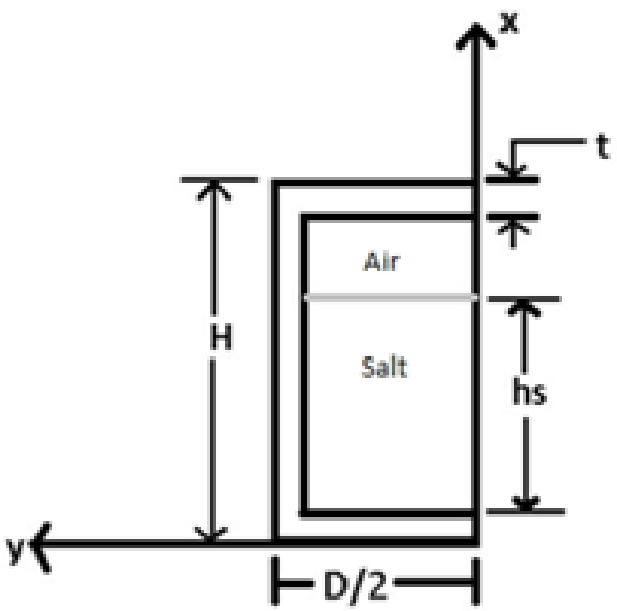

Figure 1: Cylinder schematic

CHAPTER 3: RESULTS AND DISCUSSION

3.1 Melting Results

Ten cases were analyzed for this study. The details of the cases are given in Table 1. The shape of the cylinder is varied to ascertain its effect on the melting process. The Inner Aspect Ratio (AR) is used to describe the shape of the cylinder, which is defined as the ratio of the cylinder inner height to its inner diameter. The inner volume of all cylinders is approximately constant. Due to this, while the shape of the cylinder does change, the mass of Sodium nitrate and Air in all Cases are the same. Since the same amount of Sodium nitrate is in all cylinders, the only effect on the total melting time of each cylinder is its Aspect Ratio. The effect of the Aspect Ratio also represents the effect of the Grashof Number. This number is based on a characteristic length, which is the inner diameter of the cylinder for the present study. The model under consideration has constant Stefan and Prandtl numbers across all cases, while the Grashof Number and Aspect Ratio vary. The Stefan number is fixed because the temperature difference between the initial temperature and wall temperature is fixed. The Prandtl number is fixed because the PCM material is fixed.

As can be seen from Table 1, the initial volume of solid sodium nitrate (PCM) is approximately constant across all cases. Due to this, the total melting time is only determined by the shape of the cylinder. The shape of the cylinder influences the way natural convection evolves during the melting process. Figure 2 displays the numerically predicted melt fraction

curve for first six cases. As can be seen, there is not much difference in the melting process of the first six cases. The differences may be more pronounced when the initial Sodium Nitrate mass is larger. Figure 3 displays the transient melt fraction for the last four cases. As can be seen, the AR values near and below 1 affect the total melt time the greatest. The curves in Figure 3 are not as in line as Figure 2, but a general trend still can be seen.

It will be shown that the cylinder shape influences the Velocity evolution during the melting process. High AR cases display low Velocity values initially, which gradually increases as the Melt Fraction increases. On the other hand, low AR values display high Velocity values during the entire melting process. These sustained high Velocity values cause greater heat transfer to the solid, allowing it to melt faster.

Figure 4 shows, in a compact form, the effect the AR values have on the melt time. The figure displays the aspect ratio versus the time it took to melt 99% of the PCM. It is important to note that the melt time for the cylinders increases as AR increases, but only up to a point. After this AR value, in this study this is around 4, the melt time levels off. The melt time stops increasing because the radius of the cylinder gets smaller and smaller. This decreases the thermal resistance in the radial direction. It can be seen from Figure 3 that the melt time can be reduced by almost 50% by selecting the correct Aspect Ratio. The main reason for the large difference in melt time is the natural convection within the cylinder. Figure 4 also displays a regression equation, where y is Melt Fraction Time and x is the Aspect Ratio. This regression allows to predict the melt time of cases with Aspect Ratio that were not considered in this study. It can be seen that the Aspect Ratios that affect the Melt Time, in this study, are Aspect Ratio values of 2 and below.

Initially the mode of heat transfer in the system is conduction. This always applies to the wall of the cylinder. Once inside the interior of the cylinder, the heat transfer mode at first is conduction as well. Slowly a temperature gradient begins to build within the interior volume of the cylinder as it heats up and melts. The temperature gradient also causes density differences within the fluid because the fluid's density is temperature dependent. This applies to both air and molten sodium nitrate. Natural convection starts in the air before it starts in sodium nitrate. This is because the thermal diffusivity of air is higher than that of Sodium nitrate. This allows the Air to increase in temperature faster than Sodium nitrate. During the melting process, the high convection of the Air helps melt the solid Sodium nitrate near the top of the cylinder, while this effect is more profound in low AR cases. In order to examine the natural convection, the numerically predicted temperature distribution, at different melt fractions, is shown for Cases 2 and 9 in the Figures 5 and 6 below. The velocity contours at various melt fractions of Cases 2 and 9 are shown in Figures 5 and 6 below. These two cases are chosen because they represent the two opposites in the range of AR values. In each figure, the temperature distribution is shown on the left and the stream function distribution is shown on the right. The area which has air has been colored gray for illustration.

There can be a few deductions made by observing Figures 5 and 6. The melting process in cylinders with large AR propagates mainly in radial direction. This can be seen from Figure 5, which corresponds to Aspect Ratio of 8. The melt layer can be seen by looking at the Velocity in Figure 5, which is represented by unfilled lines. The melt layer is mainly a thin radial layer for a Melt Fraction of 25%. Once the molten Sodium nitrate film layer increases in thickness, convection occurs, causing it to shape the solid Sodium nitrate. The film erodes the solid into a narrow conical shape (akin to a narrow inverted parabola). This can be easily seen looking

between Melt Fraction 50% in Figure 5. At this point, the Sodium nitrate melts slowly from top down, while maintaining the narrow conical shape, seen from Melt Fraction 75% in Figure 5. The narrowness of the conical shape was influenced by the AR, where higher AR values led to narrower conical shapes, since radius becomes smaller.

On the other hand, Case 9 in Figure 6 is seen to melt mainly top down. The solid Sodium nitrate profile of it resembles short wide inverted parabolas. Unlike Case 2 in Figure 5, the initial molten Sodium nitrate layer takes up a larger radial area. This can be seen by looking at the velocity in Figures 5 and 6 at Melt Fraction of 25%. As the melt region begins to build, it does stop primarily melting radially to primarily melting vertically. This causes the solid Sodium nitrate profile to bow out. The beginning signs of the bow can be seen at Melt Fraction of 50% in Figure 6. The effect becomes more pronounced at higher Melt Fractions, as can be seen from Figure 6.

The molten PCM velocity is influenced greatly by this difference between solid PCM shape and temperature distribution between high and low AR cases. It is thought that during melting, the large heights of high AR cases create small crossectional areas for molten PCM to flow through, causing higher velocities. The lower AR cases allow the molten salt to flow in a larger crossectional area. This larger area causes the magnitude of the velocities to decrease. From Figure 5 and 6, the maximum velocity magnitude at Melt Fraction 25% was 0.000227 kg/s and 0.000132 kg/s for Aspect Ratio of 0.48 and 8 respectively. These results show, contrary to the initial assumption, the lower Aspect Ratio cylinder allows for an effective convection of the molten Sodium nitrate in the beginning stages of the melting process. Upon closer inspection, it is found that the magnitude is lower for the higher AR case because the molten PCM is in a thin radial layer. Within this layer there is not a large temperature gradient in the vertical direction, as

seen from Figure 6, which causes slow natural convection. The gradient is mainly radial, which does not have much area for convection.

This effect is seen even at a Melt Fraction of 50%. It can be seen by comparing Figure 5 and 6, at Melt Fraction 50%, that the vertical temperature gradient is larger for Case 9 than Case 2. This effect can also be seen from the Velocity in Figures 5 and 6. For example, at Melt Fraction of 50%, the Velocity magnitude is 0.000282 kg/s and 0.000308 kg/s for Aspect Ratios of 0.25 and 8 respectively. Inspecting the vertical temperature distribution of the two cases at this melt fraction, it can be seen that there is a larger temperature gradient for Case 9 compared to Case 2 at Melt Fraction 25%. Case 2 has gotten a better temperature distribution by 50% Melt Fraction allowing its velocity to be close to that of Case 9 at 50% Melt Fraction. The molten salt layer at Melt Fraction 50% also increased radially enough to allow radial convection. The increase in the temperature gradient caused the higher velocity for Case 2. The velocity magnitude of Case 9 does exceed Case 2 at Melt Fraction 75%. At this point, the radial temperature gradient is large in Case 9 along with a large film layer. This also allows for radial circular convection as seen in Figure 6.

When examining how the velocity changes during the melting process, it can be seen from Figure 5 that low values of the velocity exist low Melt Fractions. The magnitude increases as the Melt Fraction increases up to a critical value, after which it decreases again. On the other hand, examining Figure 6, it can be seen that the velocity magnitude does not drastically change during the melting process. The velocity for Case 2 fluctuates between 0.000227 kg/s to 0.000337 kg/s during the entire melting process. For Case 9, the velocity begins at 0.000132 kg/s, increases to 0.000308 kg/s, then decreases down to 0.000243 kg/s.

It can be seen that Case 9 has the advantage compared to Case 2. The reason is the relatively constant Velocity encountered during the melting process. This shows that there is large amount of natural convection occurring within the cylinder during all Melt Fractions above 0%, causing consistent heating to the solid Sodium nitrate for Case 9. This is not the same story for Case 2. Although there is a molten film layer present at low Melt Fractions for Case 2, the primary heat transfer mode is still conduction since natural convection is not allowed to form quickly. This explains the low Velocity values at low Melt Fractions for Case 2. For Case 2, as the film layer is allowed to grow radially, natural convection is allowed to play out slowly increasing the rate of heat transfer, which can be inferred from the velocity. This is because the vertical temperature gradient becomes more profound as the film grows radially. The problem is that the peak velocity value is not reached until 50% Melt Fraction for Case 2. On the other hand, for Case 9, these high velocity values are encountered outright in the melting process.

Figure 7 displays the transient heat flux for various cases. These cases were selected to help understand the effect of cylinder shape on the melting process. One of the important things that can be seen from Figure 7 is that the Heat Flux drops dramatically initially. After this large drop, it begins to rise in magnitude by a little bit. After this increase in magnitude, the heat flux decays slowly as the melting process continues. The rise in magnitude of the heat flux after the first dramatic drop is attributed to the rise of natural convection in the system. If the natural convection was not present, the heat flux would continue to decay after its first dramatic drop. An important point to note, which can also be seen in Figure 7, is that the heat flux maintains a non-zero value even at the end of the melting process. This shows that, while the PCM has fully melted, there is still some natural convection present in the system.

Figure 8 helps understand how quick the heat penetrates to the center point of the cylinder for each case. The temperature found at this point is turned into non-dimensional form.

$$\theta = \frac{T-576.95}{579.95-576.95} \quad [7]$$

This is done through using Equation below, where T is the temperature, in Kelvin, at the center point. This non-dimensional value represents the ratio of the difference of the center point temperature from the initial temperature to the difference between the melting point temperature of Sodium Nitrate from the initial temperature. A general trend can be easily seen when inspecting Cases 2, 4, 6, 8 in Figure 8. The non-dimensional temperature increases at a very slow rate during the beginning portion of the melting process. This is expected because most of the PCM is still in the solid state. In the solid state the primary heat transfer mode is conduction. Due to this, the initial rise in temperature of the center point is minimal.

After the melting process has progress for some time, there is a quick jump in the non-dimensional temperature at the center point. The time and magnitude of this jump, and the behavior that follows is found to be a strongly affected by the cylinder shape. The occurrence of the jump happens earlier for lower Aspect Ratio cases. Cases 2, 4, and 6 in Figure 8 seem to behave very similarly after the jump in non-dimensional temperature. After the jump, there is a slow rise to the maximum value. Keep in mind that the maximum value increases as the Aspect Ratio increases, but only to a point. Cases 2 and 4 have the largest magnitude of non-dimensional temperature, around 4.25. It can be seen from this that raising Aspect Ratio above 5 does not seem to increase the maximum value of non-dimensional temperature. The higher Aspect Ratio cases undergo the jump at a later time because natural convection is not as pronounced in these cases. Due to the small radius and large heights, these cases melt from top down. There is a conical solid PCM profile, which is maintained while melting from top down. This is why the

jump in non-dimensional temperature is not seen until later, because these cases have larger heights. It takes more time for the salt to melt top down in the larger height cases.

The magnitude of the rise can also be explained by the cylinder shape. The higher AR cases do not undergo pronounced natural convection. Due to this, the heat that enters the system is not allocated evenly around the entire system. All the hot molten PCM accumulates at the top . The jump in the non-dimensional temperature helps visualize when the tip of the conical solid PCM profile decreases in height. The jump in the non-dimensional temperature is seen when this tip crosses the center point. Since the higher AR cases have hot molten fluid in a small area at the top of the cylinder, the heat of the molten fluid does not transfer into the solid salt. In addition to this, the fluid that is near the solid salt is forced upward to the top of the cylinder as it heats up, taking all the heat to the top. This can be seen in Figure 5.

The same general attributes can be seen for Case 10 in Figure 8, but the behavior after the jump in magnitude differs greatly compared to the rest of the cases. The magnitude increase of this jump for Case 10 is very small when compared to the other cases in Figure 8. Since the area at the top of the cylinder increases as the radius of the cylinder increases, the molten fluid at the top has larger heat transfer area with the solid PCM. The larger heat transfer area along with the role of natural convection allows the PCM to be heated up more. This allows the temperature of the molten fluid to be closer to the solid PCM, which decreases the magnitude of the non-dimensional temperature. This is can be seen in Figure 6. The vertical temperature gradient is more pronounced in Figure 5 than Figure 6 for this reason. A somewhat stratified temperature distribution can be seen in Figure 6, which is not as pronounced in Figure 5. This stratification is also the explanation of the behavior seen after the jump in non-dimensional temperature in

Figure 8 for Case 10. The largest magnitude of the non-dimensional temperature is still low due to the mixing and enhanced heat transfer from natural convection.

A parametric study was conducted to determine if any nondimensional variables could help in understanding the melting process. The Fourier and Grashof numbers were inspected to determine any correlations. The Aspect Ratio was also used in helping develop a correlation. The Fourier number was chosen because it is a common nondimensional number used for understanding transient heat conduction [27]. The Grashof number was chosen because it helps describe natural convection occurring within the problem. The Stefan and Prandtl numbers can also be used for the present study, but they are not included. The reason they are not included is because both the Stefan and Prandtl numbers are constant for all cases in our study.

Shatikian and others have found that the product of the Fourier and Stefan numbers do not help to account for geometrical differences [27]. Due to this, the product of the Fourier and Grashof numbers are considered. Figure 9 and Figure 10 are depicted to determine if there is a correlation between the Melt Fraction and the product of Fourier, Aspect Ratio, and Grashof numbers. There is one important thing to notice between Figures 9 and 10. The correlations developed are valid for two groups of cases. The first group, shown in Figure 9, is the first seven cases of this study. The second group, shown in Figure 10, is case 8 and 9 of this study. The correlations are developed for a group of Aspect Ratios equal to and above 1, while the later group represents Aspect Ratios below 1. Case 10 was not able to be utilized in the correlation in Figure 10. This implies that there may be a third group of cases, below Aspect Ratio of 0.48, that may have their own correlation. Since only one other data point (Aspect Ratio 0.23) is used below Aspect Ratio 0.48, the correlation in Figure 10 was not able to fit the data from Aspect Ratio 0.23.

Figures 9 and 10 also display a regression equation for each group of Aspect Ratios. For both figures, the Melt Fraction is represented by the variable y in the regression equation, and x is the product of Aspect Ratio, Fourier, and Grashof numbers. It is important to note that the exponents of the product of the dimensionless numbers vary between the two Figures. This is an important point because it reiterates the fact that multiple regressions are needed to characterize the melting behaviour across a given range of Aspect Ratios. The regression equation in Figure 9 is valid only for the Aspect Ratio range of 1 to 10, all inclusive. The regression equation in Figure 10 is only valid for the Aspect Ratio range of 0.48 to 0.77, all inclusive.

The setup of the numerical simulation was repeated using two validation cases. The first validation case is by Shmueli et. al [29]. This was done to validate the numerical model itself. The PCM and system of the validation case is slightly different than the present study. The present study investigates the melting of the PCM in a closed cylinder, while the validation case studies an open ended cylinder. Although this is the case, the numerical models and assumptions underlying the present and validation studies are very similar. Since the cylinder is open to the environment on one side, the Air in the system does not increase in pressure. Therefore, the determination of the Air density is changed from an ideal gas model to a temperature only dependent density model.

The validation case used is the experimental and numerical study by Shmueli et. al [29]. The geometry of the validation case is similar to this study. A vertical cylinder, which is open to the atmosphere on end, contains Air and a PCM. The PCM used is commercially available RT27 (Rubitherm GmbH), which has a melting interval of 26-28 ^{o}C [29]. The present simulation setup must be changed a little bit to reflect the change of an open ended cylinder. Although the simulation in this study is a closed cylinder, the open end environment can be simulated for the

air by negating the pressure influence on its density. For proper comparison with the validation case, the mushy zone constant used is 10^8. The input parameters for the validation case are detailed by Shmueli et. al [29].

Table 2 displays the comparison of the solid distribution from the numerical simulation of this study with the Validation Study. It can be seen that there is good agreement between the Present Study and the Validation Study. Commensurate with the experimental results, the initial melting occurs radially, after which it begins to melt top down. The inverted narrow parabolic solid profile is also seen in Table 2, which can be attributed to the high AR value of the Validation Study. It should be noted that the Present Study results better predict the behavior of the melting process at the bottom of the vertical cylinder. This is seen for all times in Table 2. The Validation Study does not show a curve on the bottom edge of the solid PCM, while the Present Study displays this edge. The difference of the bottom edge of the solid PCM between the Present Study and Validation Study is more profound at larger times. There is still a difference between the numerical solution and the experimental results of the Validation Study. This can be attributed to the mushy zone constant, which was found to have a large impact on the simulation results [29]. Different values of the mushy zone constant may be required at various temperature intervals for increased accuracy compared to experimental results.

The second validation study is Kalaiselvam et. al [21]. The authors studied, both experimentally and numerically, the process of solidification and melting of PCMs in cylindrical enclosure. The PCM used was 60% n-tetradecane + 40% n-hexadecane. The thermophysical properties of the PCM used is detailed by Kalaiselvam et. al [21]. The cylinder was made of copper, had a height of 350 mm and diameter of 70 mm, with a wall thickness of 1 mm. The authors studied the melting and solidification process in one dimension only. The bottom and top

of the cylinder were insulated to allow only radial propagation of the melting/solidification front. The boundary conditions on the top and bottom surface of the cylinder is changed to reflect this. The volume of fluid model is not used in the present study to simulate this validation case. The reason for this is because Kaliselvam allowed the cylinder to be filled fully with PCM. In other words, no air is present in the system. The present study uses the enthalpy-porosity to simulate the melting process of the PCM. The total time for melting in the validation study is around 7000-8000 seconds. In order to save time, the present study simulated the melting process for the first 1200 seconds. Figure 11 displays the radial position of the melting front predicted by the present study. Figure 11 also displays the experimentally determined position of the melting front during the same time interval. As can be seen from Figure 11, the present study transient melt front position resembles the validation study. There is good agreement between the two sets of data. Therefore, the numerical setup of the present study can also be used to help simulate one-dimensional melting or solidification, with the exclusion of the volume-of-fluid model.

3.2 Solidification Results

The boundary condition was changed on the final data file from the melting simulation to a temperature 10 K below the melting point of Sodium Nitrate to simulate the solidification process. In other words, the boundary condition is changed to 569.95 Kelvin. Figure 12 displays the transient melt curve for the various AR values during solidification. As can be seen, AR of a cylinder plays a important role during the solidification. During melting, it is better if the AR values are below 1, which is the opposite for solidification. Figure 12 implies that AR values above 1 are preferred during the solidification process. The solidification simulation is allowed to progress until 5% melt fraction remains. This is done to save computational time, as the last

stages of the solidification process occur, numerically, very slow. This is due to the exponential decrease of the heat flux as the solidification process continues. This is seen in Figure 15.

Figure 13 displays the temperature and velocity distribution at various melt fractions for Case 2. Figure 14 displays the same distributions for Case 9. In each figure, the temperature distribution is shown on the left and the velocity distribution is shown on the right. The area which has air has been colored pink for illustration. It can be seen, as during melting, the solidification front moves primarily in the radial direction. This is due to the large height of the cylinder. There is a large amount of natural convection occurring during the initial stages of the solidification process. This convection decreases dramatically and quickly. As can be seen from Figure 13, velocity values decrease from 0.000268 to 0.0000247 kg/s during the solidification process for Case 2. The decrease is of an order of magnitude. This effect can be seen in Figure 12. Inspecting the transient melting curve for Case 2 in Figure 12, the slope of the line decreases as time goes on. This is because the role of natural convection becomes diminished. As it becomes diminished, the heat transfer mechanism becomes conduction dominated.

Figure 14 shows the temperature distribution and velocity for Case 9. Similar results are seen in Case 9 as compared to Case 2 during solidification. The first to stand out is the velocity. The velocity in Case 9 begins at a larger value, but decreases dramatically as the solidification process progresses. There is a slight difference when compared with Case 2. The amount of decrease experienced by the velocity is larger in Case 9 than Case 2. Case 2 experienced a decrease within an order of magnitude whereas Case 9 experiences a velocity decrease greater than an order of magnitude. This causes a faster decrease in natural convection compared to Case 2, causing conduction dominated transfer mechanism. This may be attributed to the shape of the cylinder. The AR value of Case 9 is low, allowing the fluid to disperse itself radially. Case 2

cannot do this due to its small radius. As expected, this effect can be seen in Figure 12. Case 9 in Figure 2 shows a larger decrease in slope compared to Case 2. This causes slower and slower heat transfer, causing the large solidification time.

Figure 15 compares the solidification front for Case 2 and 9 at various melt fractions. Case 2 is on the left and Case 9 is on the right. The area occupied by air is also shown in Figure 15 in pink color. Similar solid-liquid interface profiles are found during solidification as in the melting process. The only difference is that the profiles are inverted vertically. While these general trends can be seen during the melting and solidification process, the effect of natural convection is much more drastic. Natural convection depends on the temperature differences that exist within the liquid medium. These temperature gradients are not found during the solidification process in Figure 13 and 14. It can be seen that the entire molten region is around 579 K. As the solidification process continues, the temperature gradients decrease further and further. The decrease of these gradients causes dramatic decreases in the velocity. This reduced velocity is reduced natural convection. This causes the heat transfer mechanism to be primarily conduction as the solidified salt layer builds from the wall towards the center.

The effect of this decrease in velocity can also be seen in Figure 16, which displays the transient heat flux at the inner wall for various cases. It can be seen from Figure 16 that regardless of the aspect ratio, the behavior of the transient heat flux is similar. The reason for this is because the primary heat transfer mechanism in solidification is conduction. Conduction alone is less effective at transferring heat when compared with conduction and natural convection. As the solidified layer builds from the walls to the center of the cylinder, the conduction thermal resistance increases proportionally. In addition to this, the natural convection becomes diminished as the solidification process continues. Due to this, the heat flux gradually decreases

during the entire process at an exponential rate. The effect of natural convection is easily noticeable when comparing Figure 16 and Figure 7. In Figure 7, the magnitude of heat flux has a dramatic drop at the beginning, after which it is followed by an increase. This increase is ascribed to natural convection. In Figure 16, it can be seen that after the dramatic drop in magnitude, the heat flux continues to decrease.

Figure 17 helps understand how the Aspect Ratio affects the solidification time. The time displayed is the time required to achieve 95% solidification. Figure 17 shows that higher Aspect Ratio cases decrease the solidification time the greatest. There is a large drop in solidification time when comparing Aspect Ratio 0.48 and 0.77, but this is not as pronounced as the reduction in solidification time at high Aspect Ratios. Aspect Ratio of 10 indicates a 60% reduction in solidification time compared to the maximum solidification time of 1937 seconds of Case 8. This is easily seen in Figure 18. A possible future study can be studying solidification times of Aspect Ratios below 0.23 to see if a 60% reduction of max solidification time is achievable. If this is achievable, it will be possible to use a cylinder shape that allows for both fastest melting and solidification processes. If this is not achievable, it may not be a bad scenario.

Figure 18 displays the percent reduction of time of each case as compared to the maximum solidification and melting times. The cases with Aspect Ratio of 0.23 and 0.48 are not shown in Figure 18 because the reduction in solidification time is not high. The maximum solidification time is 1937 seconds from Case 8, and the maximum melting time is 260 seconds from case 1. It is important to note that the maximum melting time is with reference to the melting time required to achieve 99% melt fraction in Figure 4.

Figure 18 also displays regressions for both the solidification and melting curves. These regressions describe the Aspect Ratio effect on the reduction in maximum solidification and

melting time. These regressions are valid for an Aspect Ratio Range of 0.77 to 10. An interesting observation is that these curves intersect at an Aspect Ratio 1.32. If the assumption that Aspect Ratios below 0.23 do not reduce the maximum solidification time more than 60%, then Figure 18 can be used to reach an important conclusion. The conclusion is that Aspect Ratios above 6 are preferred for both solidification and melting processes. This conclusion is contrary to what is found in the melting study but supersedes the conclusion of the melting study. The maximum solidification time is an order of magnitude higher than the maximum melting time. Therefore the percentages on shown in Figure 18 are of more importance to the solidification process than the melting process. While the high Aspect Ratios have high melting times, the amount of time saved in solidification greatly outweighs the increase in melting time. Keep in mind this is valid only if Aspect Ratios below 0.23 do not decrease the max solidification time 60% or more.

Table 1: Details of cylinder cases

Case	D_i (mm)	H_i (mm)	Gr #	AR	h_s (mm)	V_{na} (m^3)
1	20	200	2.15E+05	10.00	149.4	4.694E-05
2	21.5	173	2.68E+05	8.05	129.3	4.694E-05
3	23.7	142.5	3.58E+05	6.01	106.4	4.694E-05
4	25.2	126	4.31E+05	5.00	94.1	4.693E-05
5	27	109.7	5.30E+05	4.06	82	4.695E-05
6	34	69.2	1.06E+06	2.04	51.7	4.694E-05
7	43.1	43.1	2.16E+06	1.00	32.2	4.698E-05
8	47	36.2	2.80E+06	0.77	27.05	4.693E-05
9	55	26.50	4.48E+06	0.48	19.8	4.704E-05
10	70	16.35	9.24E+06	0.23	12.21	4.699E-05

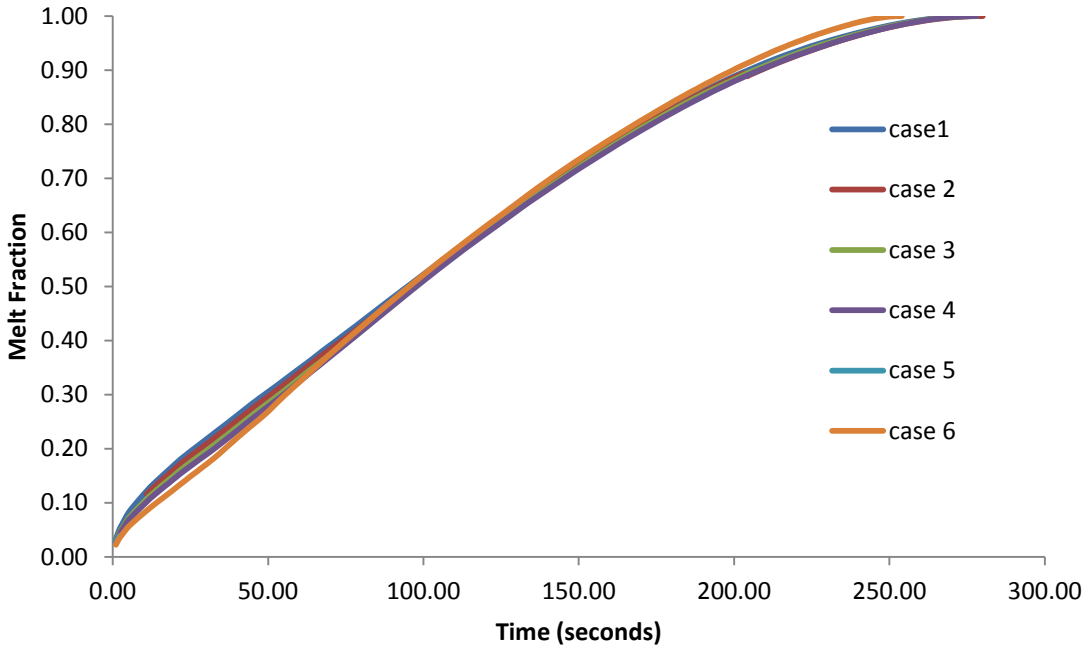

Figure 2: Transient melt fraction of first six cases.

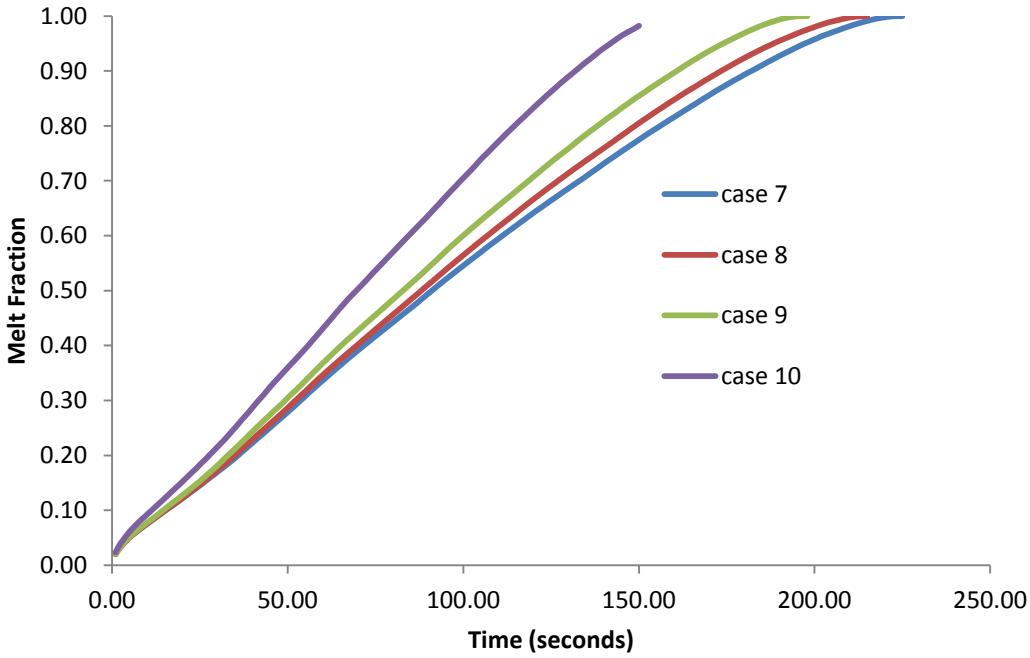

Figure 3: Transient melt fraction of last four cases

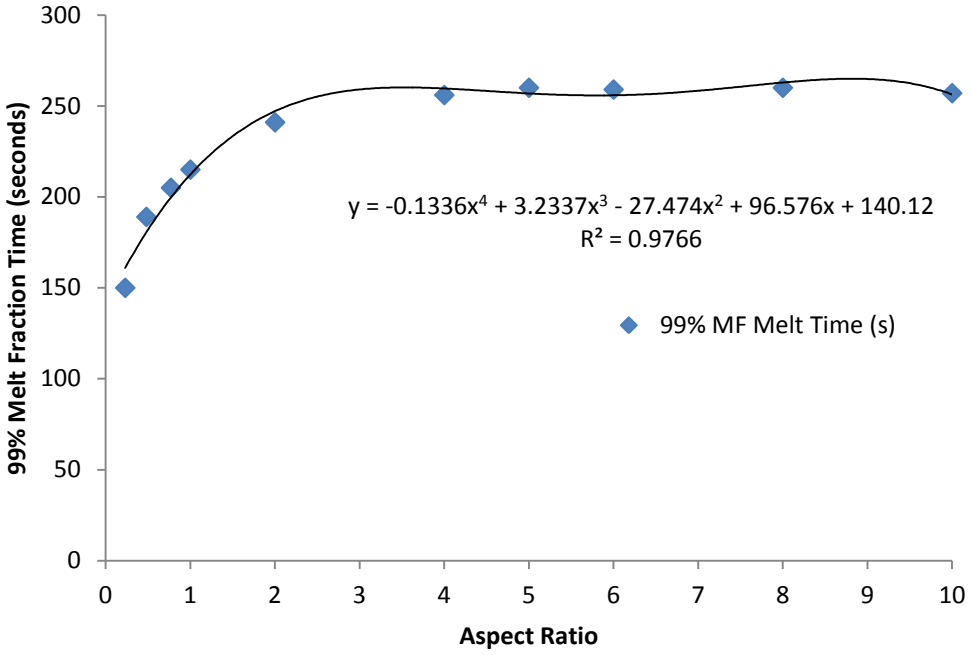

Figure 4: Melt time vs aspect ratio

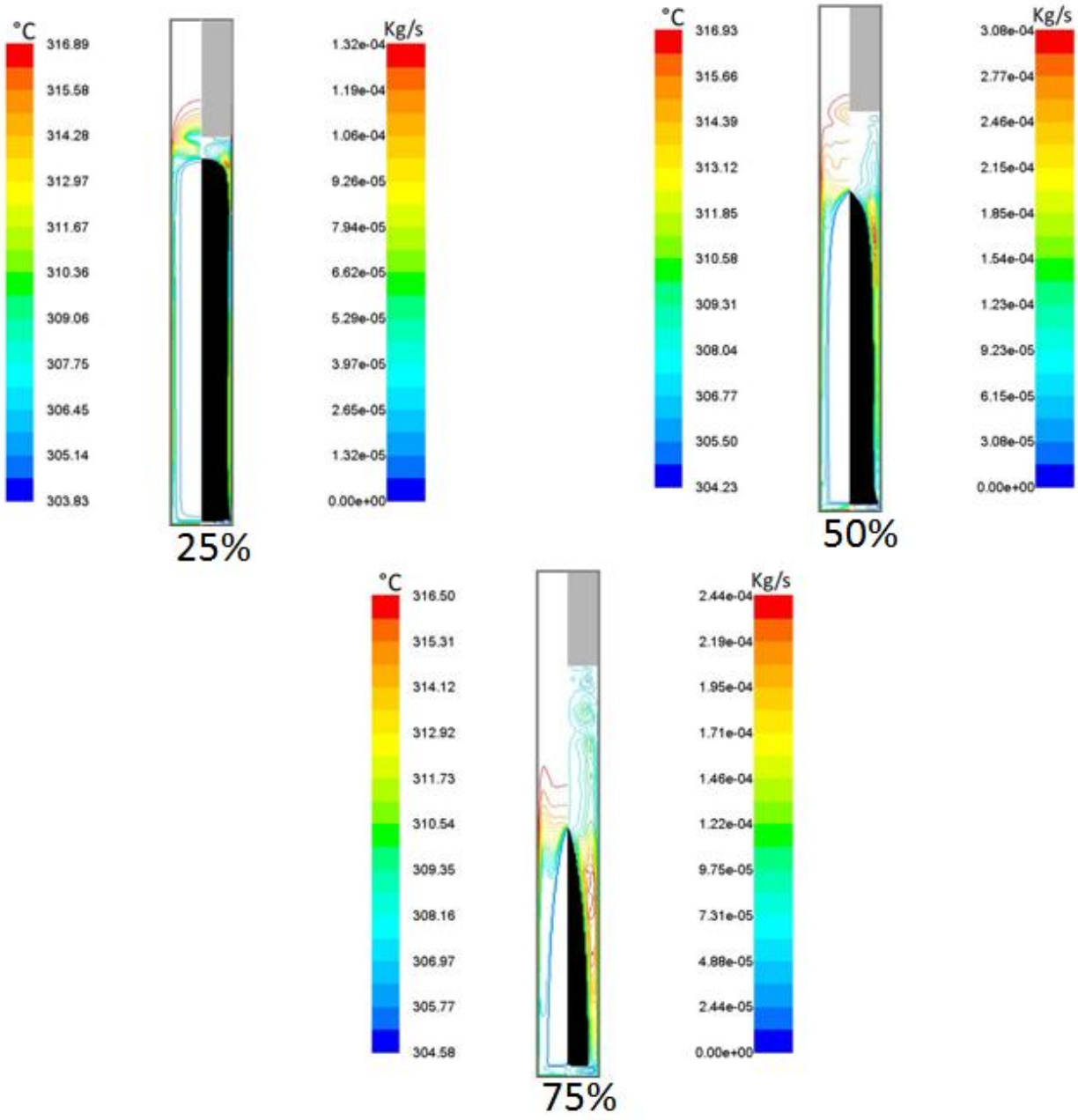

Figure 5: Case 2 stream function and temperature distribution contours at various melt fractions

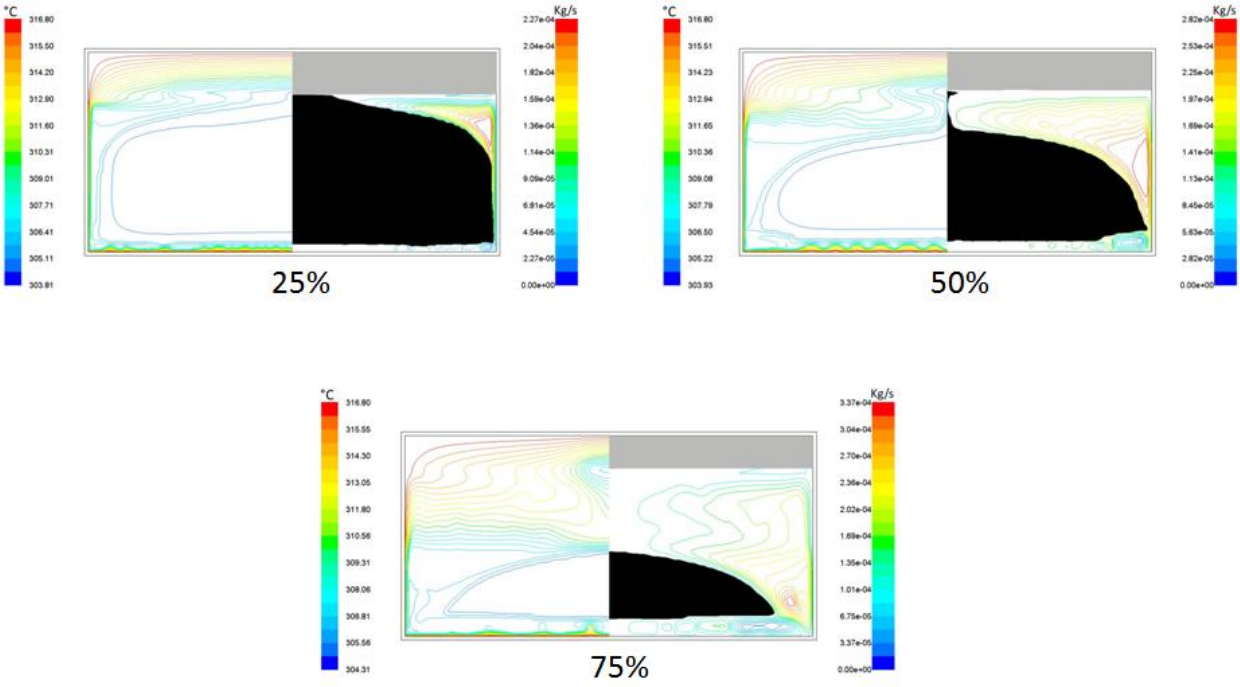

Figure 6: Case 9 stream function and temperature distribution contours at various melt fractions

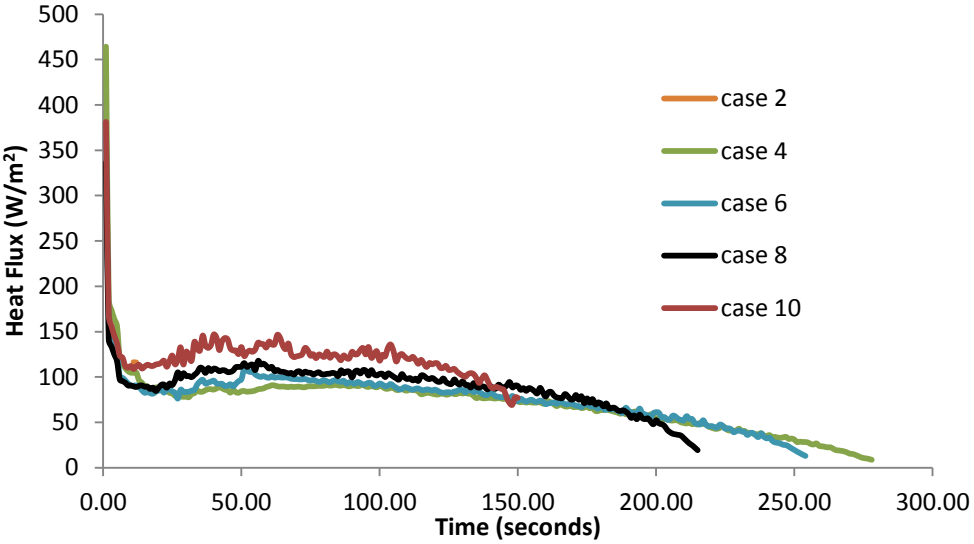

Figure 7: Transient heat flux of various cases during melting

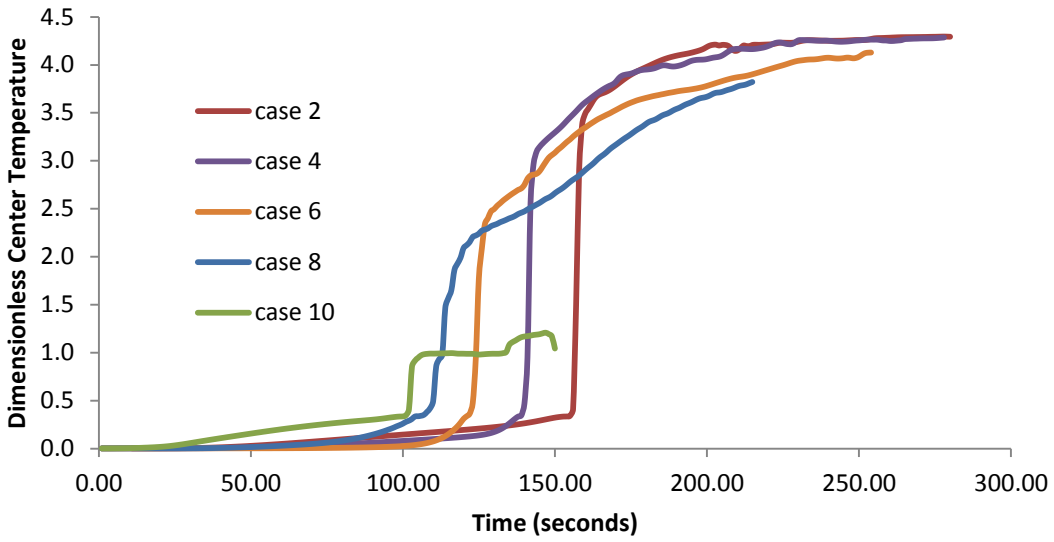

Figure 8: Distribution of θ for various cases

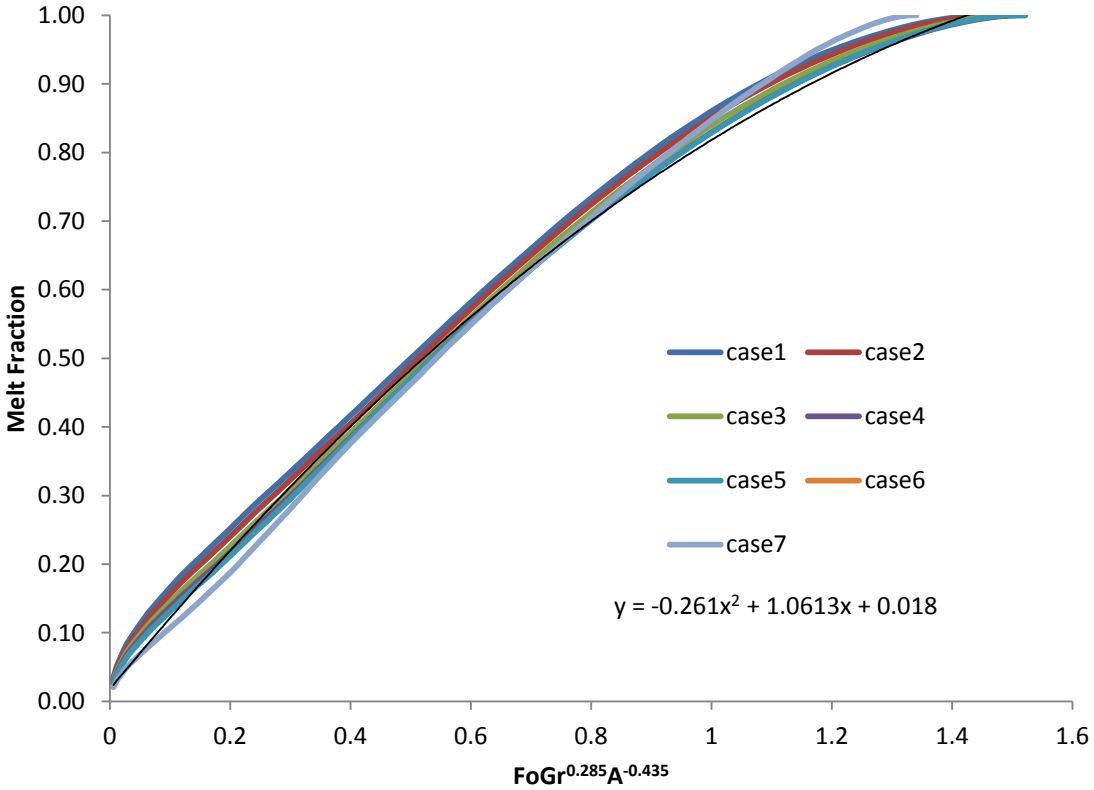

Figure 9: Dimensionless transient melt fraction of first seven cases

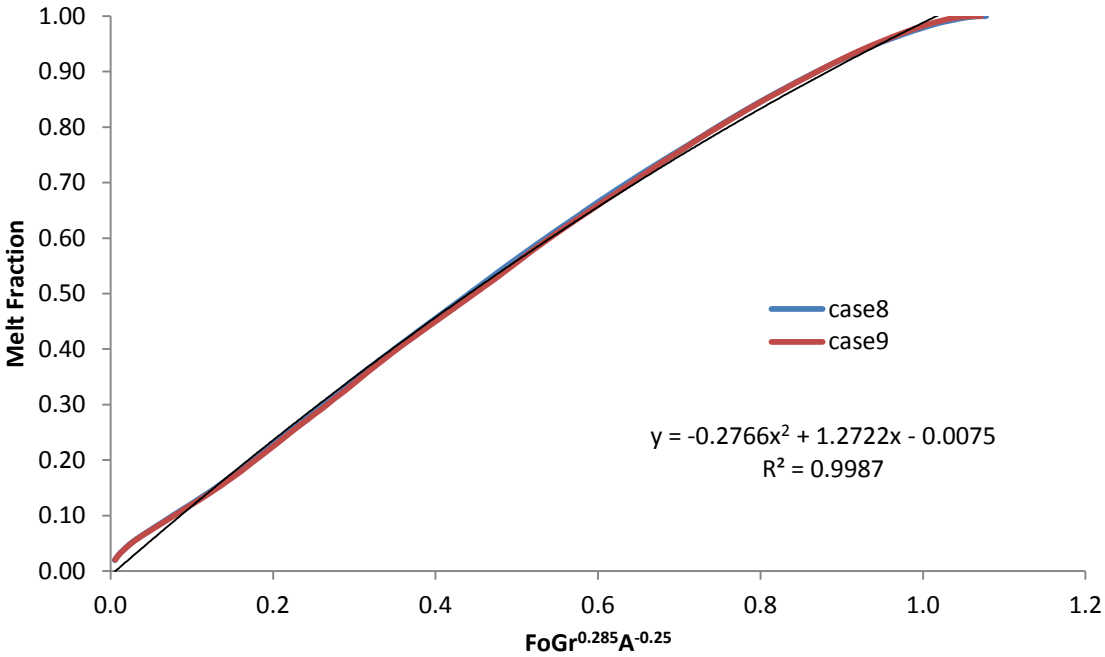

Figure 10: Dimensionless transient melt fraction of cases 8 and 9

Table 2: Simulation results-present study vs validation study [29]

Time (min)	Present Study	Validation Study [29]
8	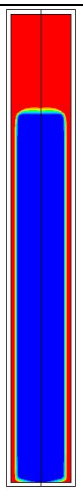	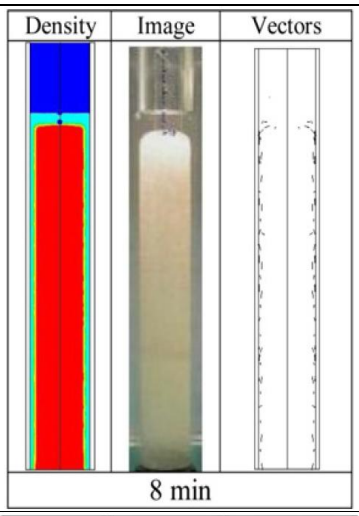
16	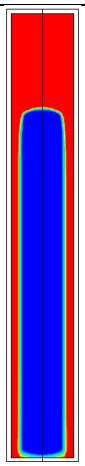	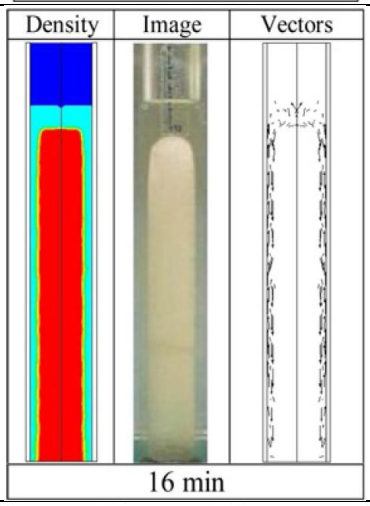
32	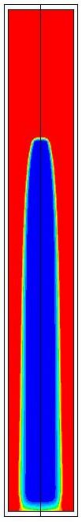	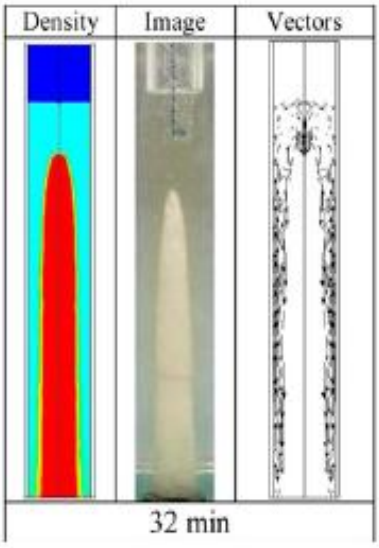

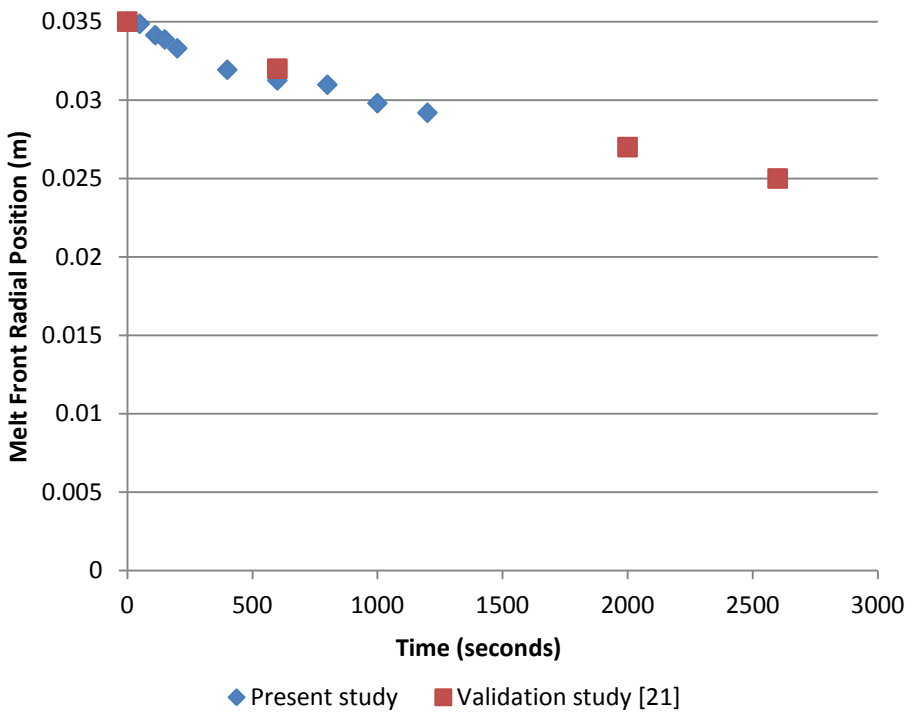

Figure 11: Comparison with validation study [21]

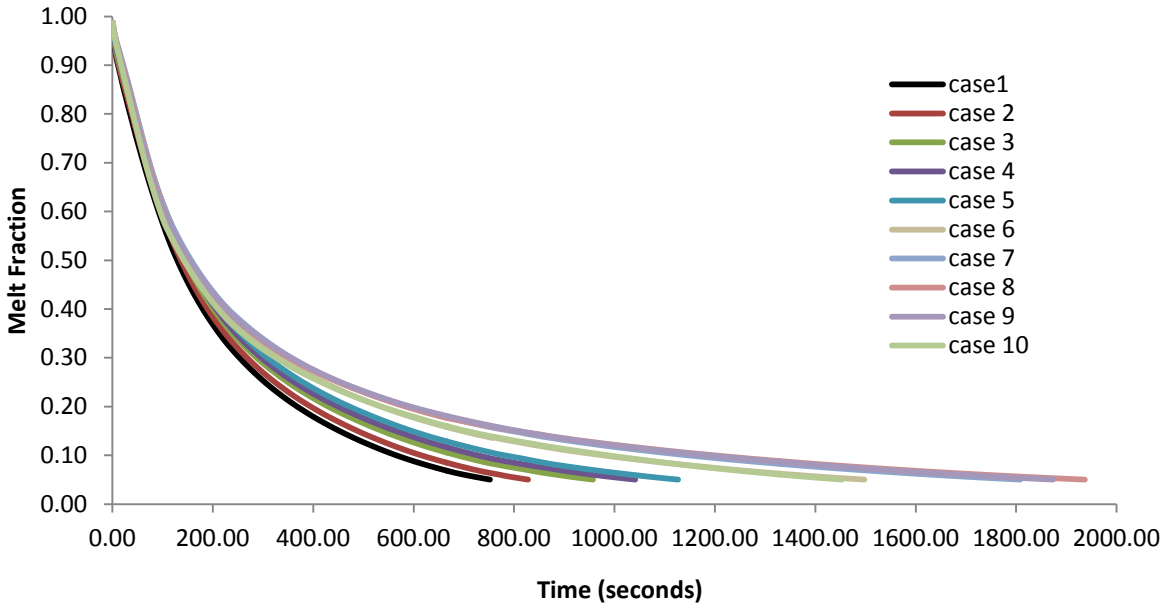

Figure 12: Transient melt fraction of various cases during solidification

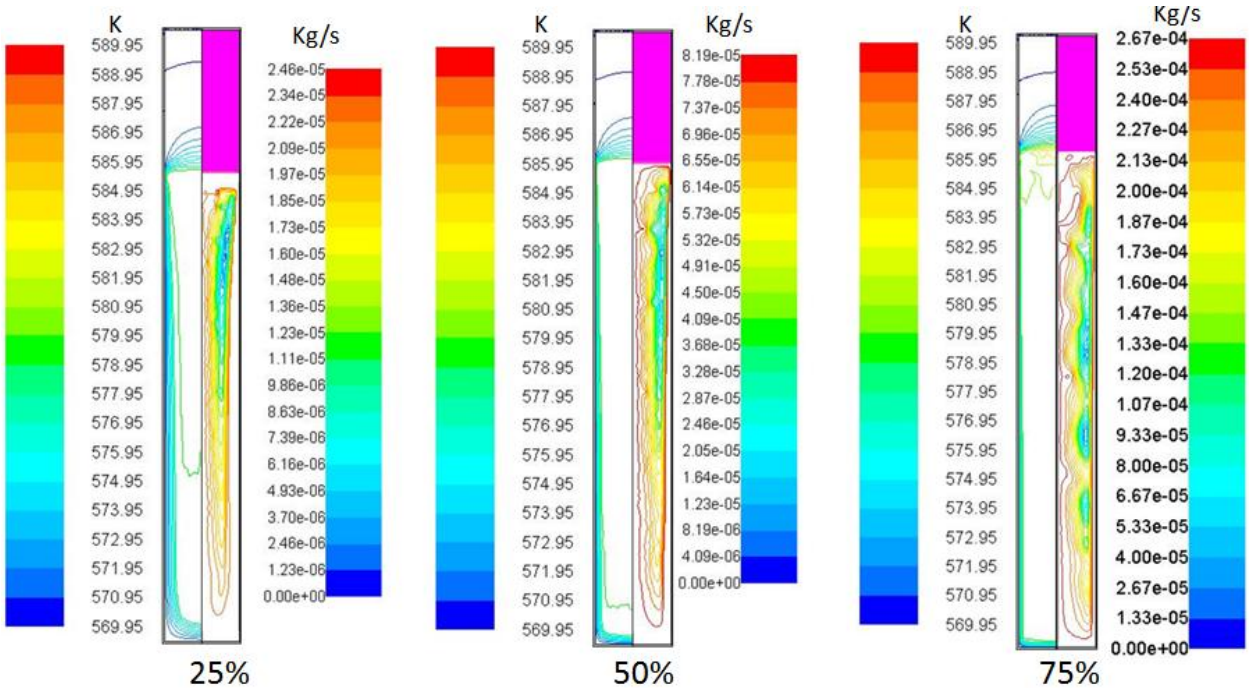

Figure 13: Case 2 temperature distribution and stream function contours at various melt fractions during solidification

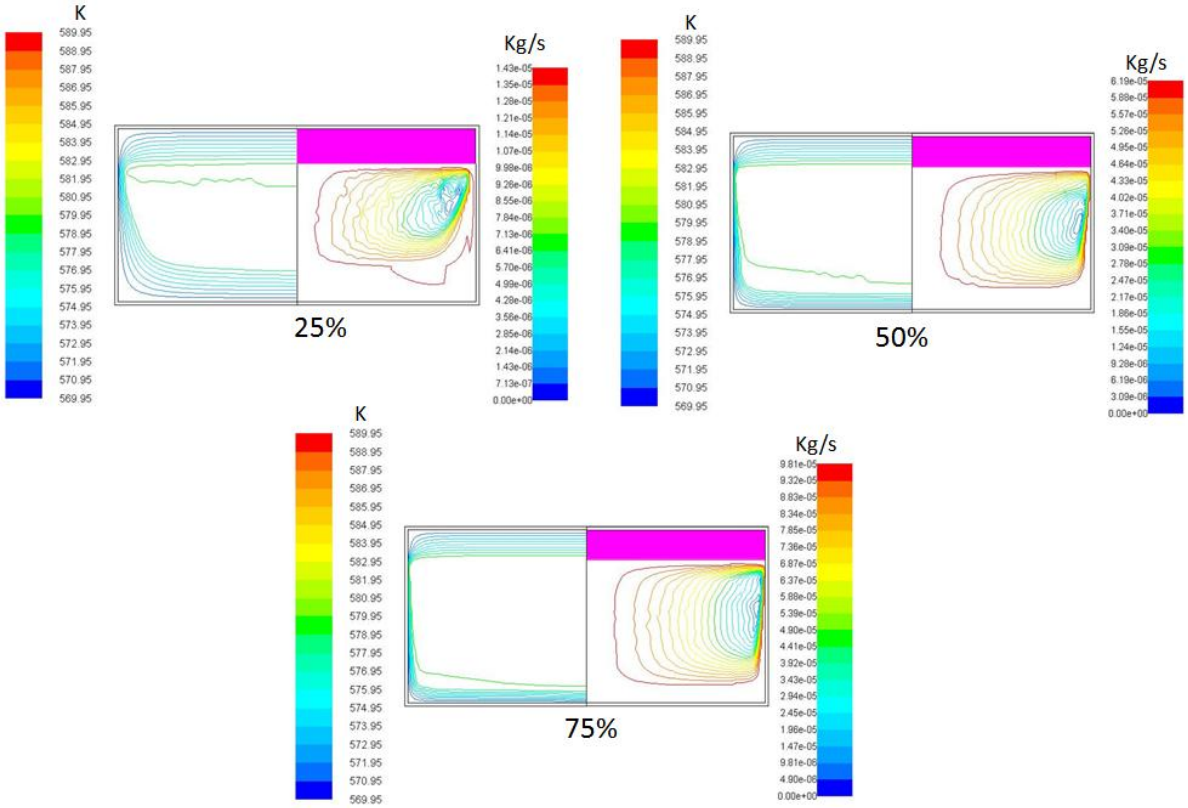

Figure 14: Case 9 temperature distribution and stream function contours at various melt fractions during solidification

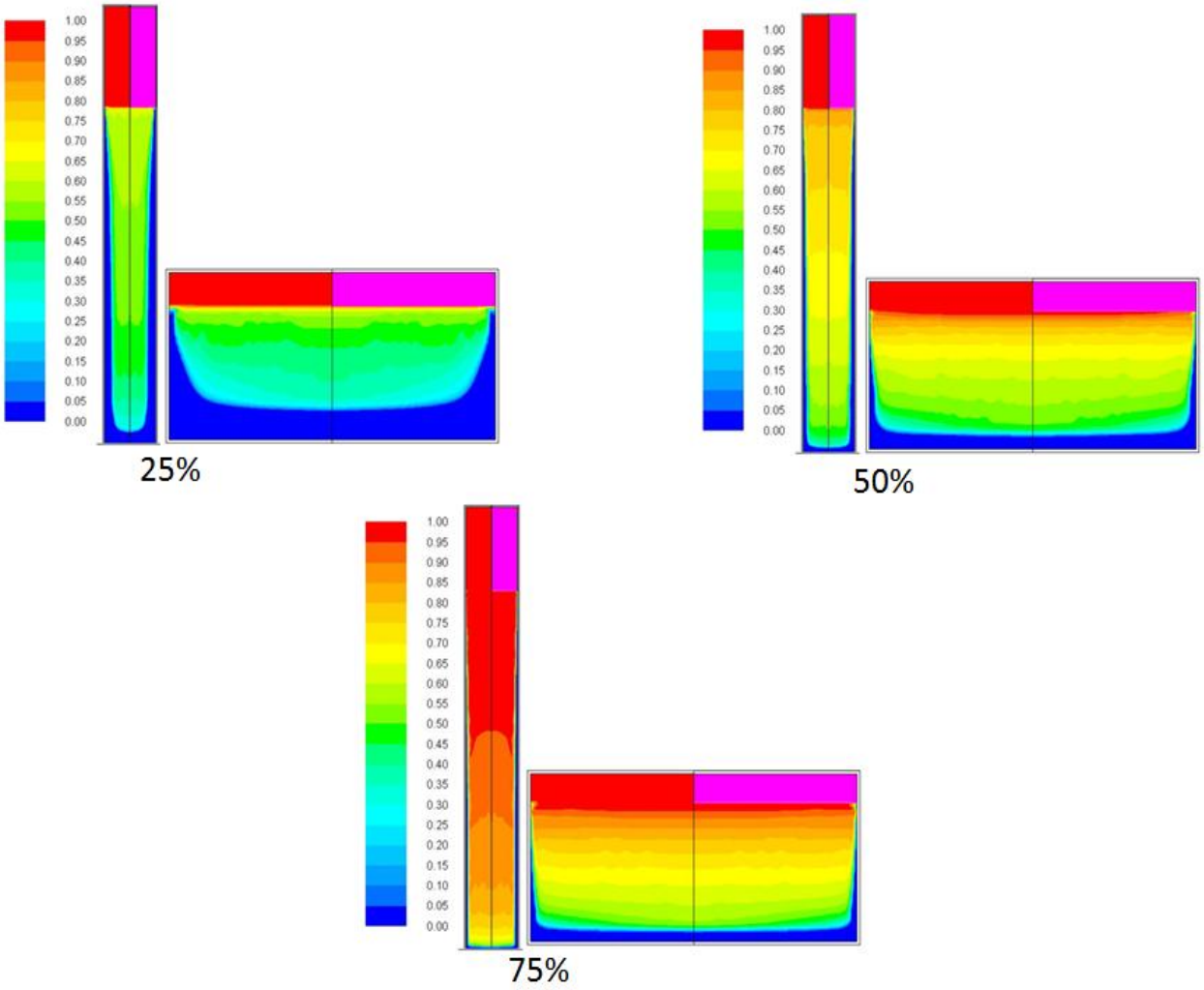

Figure 15: Case 2 and 9 melt distribution at various melt fractions during solidification

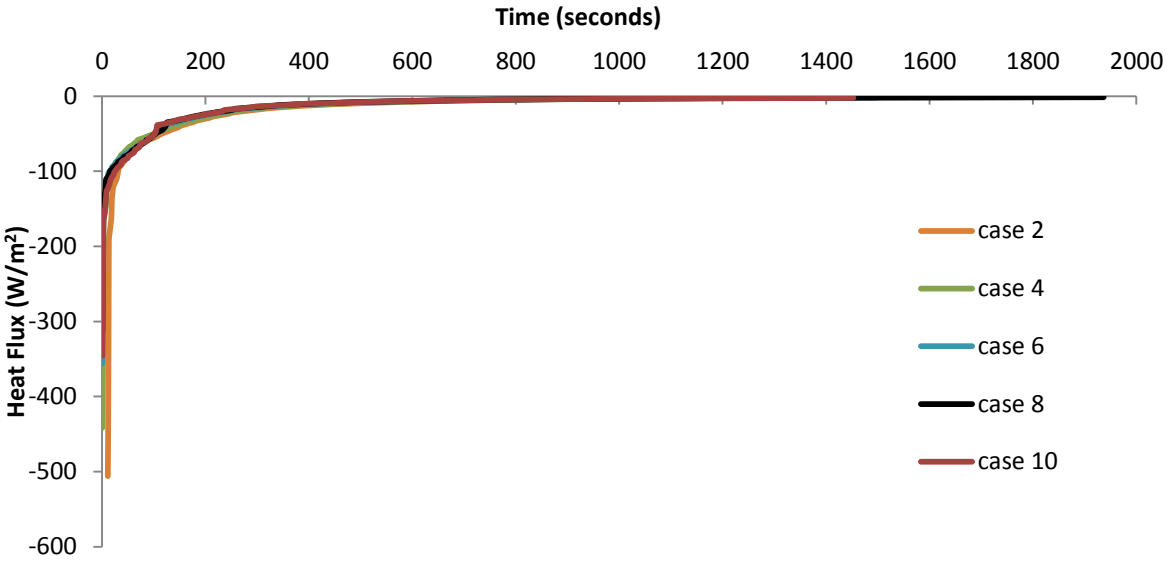

Figure 16: Transient heat flux curve during solidification

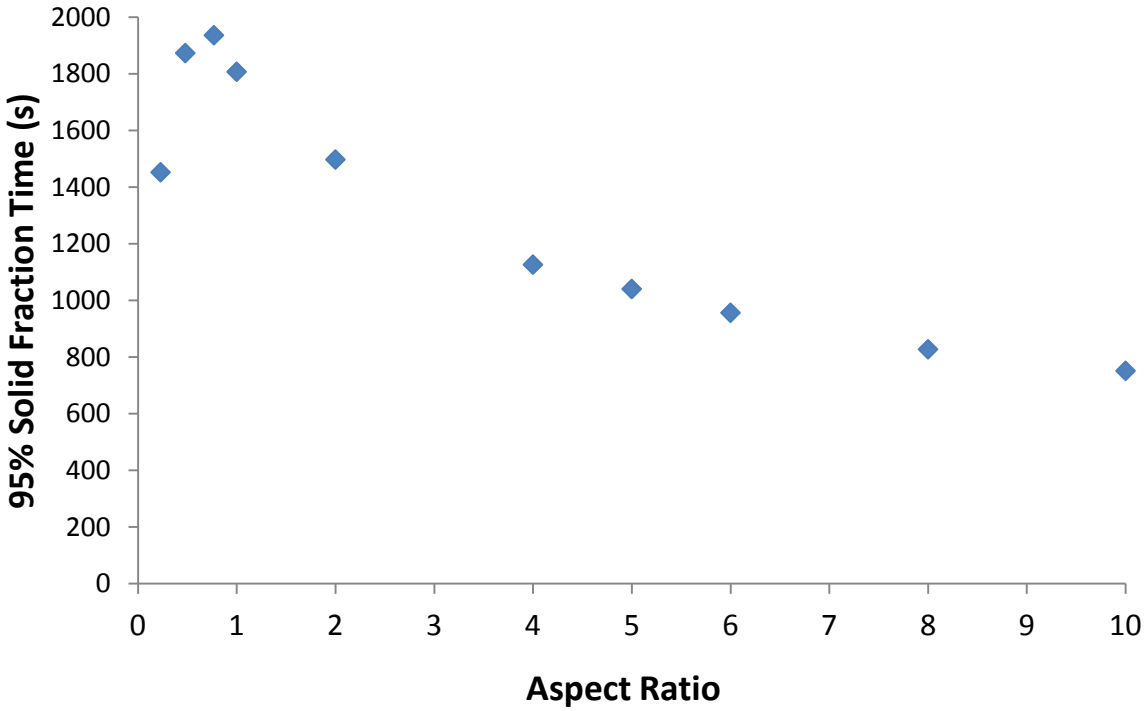

Figure 17: 95% solid fraction time vs aspect ratio

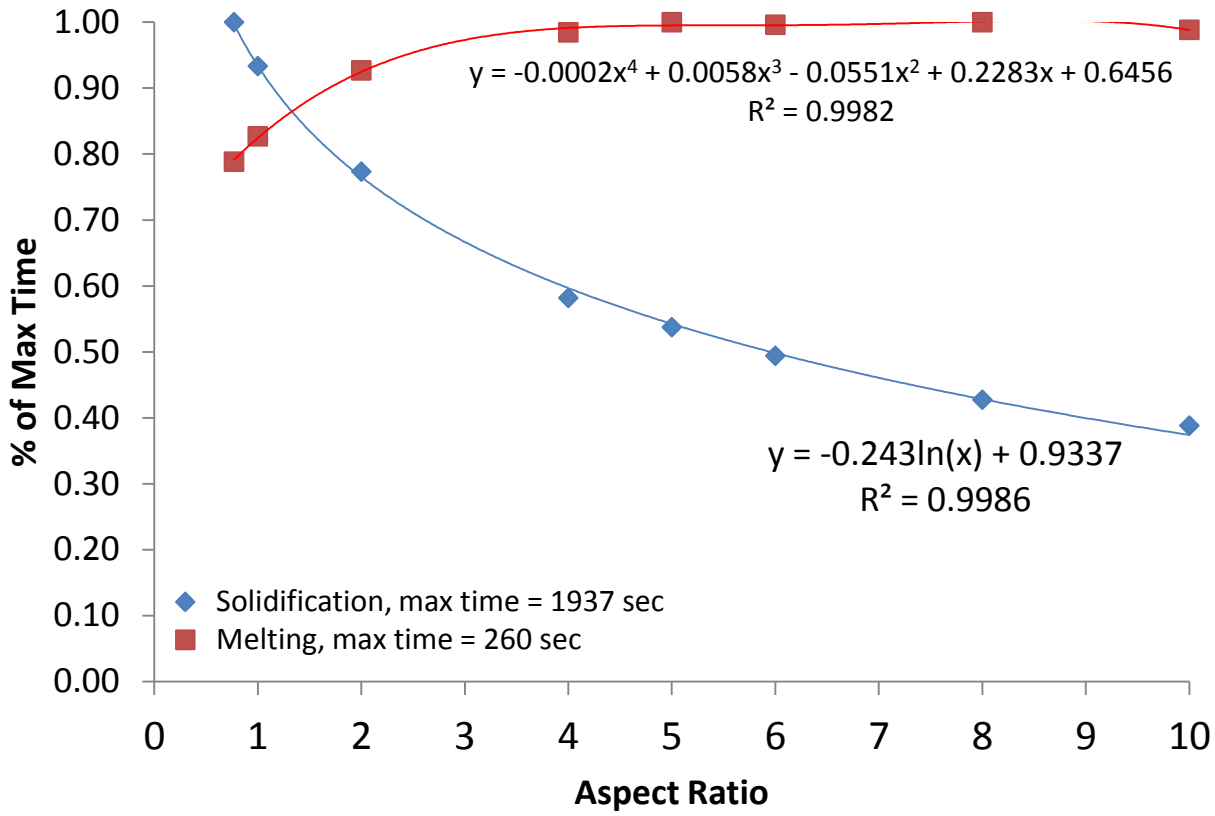

Figure 18: Percent of max time vs aspect ratio

CHAPTER 4: CONCLUSIONS

A numerical simulation of the heat transfer and fluid flow during the melting and solidification processes of Sodium Nitrate in a cylindrical container is shown. The mass of Sodium Nitrate is held constant while the shape of the cylinder is changed. The effect of the shape of the cylinder on the melting and solidification process is determined. The volume-of-fluid model is used to track the interface between Sodium Nitrate and air. Utilizing this model, the compression of the air during the melting process is shown by tracking the interface movement. The following conclusions can be drawn:

It was found that the shape of the cylinder greatly impacts the melting process. This was determined by examining the Grashof Number and Aspect Ratio (AR), both of which depend on the shape of the cylinder. The Grashof number increases as AR decreases. It was found that low AR values contribute to lower melting times compared to high AR values. It was found that the melting time does not change significantly as high AR values are approached. It was found that AR values below 1 were necessary for the quickest melting times.

The shape of the cylinder affected the velocity evolution during the melting process. High AR values attributed to low velocities at initial stages of the melting process. As the Melt Fraction increased, the velocity of these cases gradually increased. It was found that the peak values occurred around 75% Melt Fraction. On the other hand, low AR values caused high

velocity values for all Melt Fractions. These higher values caused greater heat transfer to the solid, allowing it to melt faster.

It was found that the shape of the cylinder greatly impacts the solidification process. This was determined by examining the Grashof Number and Aspect Ratio (AR), both of which depend on the shape of the cylinder. It was found that low AR values contribute to longer solidification times compared to high AR values. It was found that AR values above 5 were necessary for the quickest solidification times.

During solidification, the velocity decreased dramatically regardless of the AR value. The AR value did affect the amount of decrease of velocity during the solidification process. High AR values caused slower decreases of velocities causing quicker solidification compared with low AR values. Conduction was the primary heat transfer mechanism during solidification.

The numerical simulation was redone to repeat the results of a validation case. The numerical results of the present study resembled the numerical results of the validation case, but discrepancy existed when compared to the experimental results of the validation case. This discrepancy was attributed to the mushy zone constant, but further work is needed for accurate determination. The best Aspect Ratio to be used is above 5 because these Aspect Ratios decrease the maximum solidification time the most. Since the maximum solidification time is an order of magnitude higher than the maximum melting time, higher Aspect Ratio cylinders are preferred for both the melting and solidification process.

REFERENCES

[1] Al-Abidi A. A, Mat S, Sopian K, Sulaiman M. Y, Mohammad A. T. Numerical study of PCM solidification in a triplex tube heat exchanger with internal and external fins. *International Journal of Heat and Mass Transfer*. 2013; 61: pp.684-695.

[2] Alawadhi E. M. A solidification process with free convection of water in an elliptical enclosure. *Energy Conversion and Management*. 2009; 50: pp.360-364.

[3] Assis E, Katsman L, Ziskind G, Letan R. Numerical and experimental study of melting in spherical shell. *International Journal of Heat and Mass Transfer*. 2007; 50: pp.1790-1804.

[4] Bauer T. Approximate analytical solutions for the solidification of PCMs in fin geometries using effective thermophysical properties. *International Journal of Heat and Mass Transfer*. 2013; 54: pp.4923-4930.

[5] Bauer T, Laing D, Kröner U, Tamme R. Sodium Nitrate for high temperature latent heat storage. *11th Conference on Thermal Energy Storage*. 14-17 June, Stockholm, Sweden, 2009.

[6] Bilir L, Ilken Z. Total solidification time of a liquid phase change material enclosed in cylindrical/spherical containers. *Applied Thermal Engineering*. 2005; 25: pp.1488-1502.

[7] Cho K, Choi S.H. Thermal characteristics of a paraffin in a spherical capsule during freezing and melting processes. *International Journal of Heat and Mass Transfer*. 2000; 43: pp.3183-3196.

[8] Eames W. I, Adref T. K. Freezing and melting of water in spherical enclosures of the type used in thermal (ice) storage systems. *Applied Thermal Engineering*. 2002; 22: pp.733-745.

[9] El Omari K, Kousksou T, Le Guer Y. Impact of shape of container on natural convection and melting inside enclosures used for passive cooling of electronic devices. *Applied Thermal Engineering*. 2011; 31: pp.3022-3035.

[10] Farid M. M, Khudhair A. M, Razack S. A. K, Al-Hallaj S. A review on phase change energy storage: materials and applications. *Energy Conversion and Management*. 2004; 45: pp.1597-1615

[11] Faraji M, El Qarnia H. Numerical study of melting in an enclosure with discrete protruding heat sources. *Applied Mathematical Modeling*. 2010; 34: pp.1258-1275.

[12] Guo C, Zhang W. Numerical simulation and parametric study on a new type of high temperature latent heat thermal energy storage system. *Energy Conversion and Management.* 2008; 49: pp.919-927.

[13] Hasnain S. M. Review on sustainable thermal energy storage technologies, part 1: heat storage materials and techniques. *Energy Conversion and Management*. 1998; 39: pp. 1127-1138

[14] Hoshi A, Mills D. R, Bittar A, Saitoh T. S. Screening of high melting point phase change materials (PCM) in solar thermal concentrating technology based on CLFR. *Solar Energy.* 2005; 79: pp.332-339

[15] Hosseini M. J, Ranjba A. A, Sedighi K, Rahimi M. A combined experimental and computational study on the melting behavior of medium temperature phase change storage material inside shell and tube heat exchanger. *International Communications in Heat and Mass Transfer*. 2012; 39: pp.1416-1424.

[16] Hosseinizadeh S.F, Tan F.L, Moosania S.M. Experimental and numerical studies on performance of PCM-based heat sink with different configurations of internal fins. *Applied Thermal Engineering*. 2011; 31: pp.3827-3838.

[17] Ibrahim B. M, Ahn H. K. Transient thermal analysis of phase change process. *Transport Phenomena in Heat and Mass Transfer*. 1992.

[18] Ismail K.A.R, Moraes R.I.R. A numerical and experimental investigation of different containers and PCM options for cold storage modular units for domestic applications. *International Journal of Heat and Mass Transfer.* 2009; 52: pp.4195-4202.

[19] Ismail K.A.R, Henriquez J.R. Solidification of PCM inside a spherical capsule. *Energy Conversion and Management.* 2000; 41: pp.173-187.

[20] Ismail A. R. Kamal, Maria das Gracas E. da Silva. Melting of PCM around a horizontal cylinder with constant surface temperature. *International Journal of Thermal Sciences*. 2003; 42: pp.1145-1152

[21] Kalaiselvam S, Veerappan M, Arul Aaron A, Iniyan S. Experimental and analytical investigation of solidification and melting characteristics of PCMs inside cylindrical encapsulation.

[22] Kim Y, Hossain A, Nakamura Y. Numerical study of melting of a phase change material enhanced by deformation of a liquid-gas interface. *International Journal of Heat and Mass Transfer*. 2013; 63: pp.101-112.

[23] Medrano M, Gil A, Martorell I, Potau X, Cabeza L. F. State of the art review on high-temperature thermal energy storage for power generation, part 2- case studies. *Renewable and Sustainable Energy Reviews.* 2010; 14: pp. 56-72.

[24] Nunes, V. M. B, Lourenço M. J. V, Santos F. J. V, Nieto de Castro C. A. Viscosity of molten Sodium Nitrate. *Int J Thermophys*. 2006; 27: pp. 1638-1648

[25] Patankar V. Suhas. Numerical Heat Transfer and Fluid Flow. McGraw-Hill 1980.

[26] Ramachandran N., Gupta J. P., Jaluria Y. Thermal and fluid flow effects during solidification in a rectangular enclosure. *International Journal of Heat and Mass Transfer*. 1982; vol. 25: pp.187-194.

[27] Shatikian V., Ziskind G., Letan R. Numerical investigation of a PCM-based heat sink with internal fins. *International Journal of Heat and Mass Transfer*. 2005; 48: pp.3689-3706

[28] Shih Y, Chou T. Analytical solutions for freezing a saturated liquid inside or outside spheres. Analytical solutoins for freezing a saturated liquid inside or outside spheres. *Chemical Engineering Science*. 1971; 26: pp.1787-1793.

[29] Shmueli H, Ziskind G, Letan R. Melting in vertical cylinder tube: numerical investigation and comparison with experiments. *International Journal of Heat and Mass Transfer*. 2010; 53: pp.4082-4091.

[30] Tan F.L., Hosseinizadeh S.F., Khodadadi J.M., Fan Liwu. Experimental and computational study of constrained melting of phase change materials (PCM) inside a spherical capsule. *International Journal of Heat and Mass Transfer*. 2009; 52: pp.3464-3472.

[31] Tan H, Li C, Li Y. Simulation research on PCM freezing process to recover and store the cold energy of cryogenic gas. *International Journal of Thermal Sciences*. 2011; 50: pp.2220-2227.

[32] Trp A. An experimental and numerical investigation of heat transfer during technical grade paraffin melting and solidification in a shell-and-tube latent thermal energy storage unit. *Solar Energy* 2005; 79: pp. 648-660.

[33] Velraj R., Seeniraj R. V., Hafner B., Faber C., Schwarzer K. Experimenal analysis and numerical modeling of inward solidification on a finned vertical tube for a latent heat storage unit. *Solar Energy*. 1997; 60: pp.281-290.

[34] Voller V. R, Prakash C. A fixed grid numerical modelling methodology for convection-diffusion mush region phase-change problems. *International Journal of Heat and Mass Transfer*. 1987; 30: pp.1709-1719.

[35] Wyman C, Castle J, Kreith F. A review of collector and energy storage technology for intermediate temperature applications. *Solar Energy.* 1980; 24: pp.514-540.

[36] Ye W, Zhu D, Wang N. Fluid flow and heat transfer in a latent thermal energy unit with different phase change material (PCM) cavity volume fractions. *Applied Thermal Engineering.* 2012; 42: pp.49-57.

[37] Zhang X, Fujii M. Simultaneous measurements of thermal conductivity and thermal diffusivity of molten salts with a transient short-hot-wire method. *Int J Thermophys*. 2000; 21: pp.71-83.

[38] Zhao W, Neti S, Oztekin A. Heat transfer analysis of encapsulated phase change materials. *Applied Thermal Engineering*. 2012; doi:10.1016/j.applthermaleng.2012.06.016.

APPENDICES

Appendix A Nomenclature

A_i	inner cylinder surface area (m^2)
AR	aspect ratio (H/D)
C_p	specific heat of PCM (J/kg-K)
D	outer diameter of cylinder (m)
D_i	inner diameter of cylinder (m)
Gr	Grashof number $(g\beta(T_w - T_m)(2R_i)^3\nu^{-2})$
h	sensible enthalpy (J/kg)
$\hbar_i$	enthalpy of i-th fluid (J/kg)
h_s	salt/interface height (m)
H	outer height of cylinder (m)
HH	total enthalpy (J/kg)
H_i	inner height of the cylinder (m)
ΔH	latent heat enthalpy (J/kg)
L	latent heat of phase change (J/kg)
P	pressure (Pa)
PCM	phase change material
Pr	Prandtl number (ν/α)
R_i	inner radius of the cylinder (m)
Ste	Stefan number $(C_p(T_w - T_m)/L)$
t	wall thickness of cylinder (m)
T	temperature (K)
$T_{liquidus}$	liquidus temperature (K)
T_m	melting temperature (K)
$T_{solidus}$	solidus temperature (K)
T_w	wall temperature (K)
u_i	velocity of i-th fluid (m/s)
V_i	inner cylinder volume (m^3)
V_{na}	salt volume (m^3)

Greek symbols

α_i	volume fraction of i-th fluid
θ	center point dimensionless temperature (K) $((T - 576.95)/(579.95 - 576.95))$
κ_i	thermal conductivity of i-th fluid (W/(m-K))
μ	dynamic viscosity (kg/(m-s))
ρ_i	density of i-th fluid (kg/m^3)
ν	kinematic viscosity (m^2/s)